THE PREPARATION , CHARACTERIZATION AND SINTERING OF NANOCRYSTALLINE CERAMICS

Özlem ÇAĞLAR

September , 1999

The Preparation, Characterization and Sintering of Nanocrystalline Ceramics

By
Özlem ÇAĞLAR

A Dissertation Submitted to the

Graduate School in the Partial Fulfillment of the

Requirements for the Degree of

MASTER OF SCIENCE

Department: Materials Science and Engineering

Major: Materials Science and Engineering

Izmir Institute of Technology

Izmir, Turkey

September 1999

We approve the thesis of Özlem CAĞLAR

Date of Signature

[signature]
....   29.09.99
Prof. Dr. Muhsin ÇİFTÇİOĞLU
Supervisor
Department of Chemical Enginnering

[signature]
....   29.09.99
Assist. Prof. Dr. Funda TIHMINLIOĞLU
Department of Chemical Engineering

[signature]
....   29.09.99
Assoc. Prof. Dr. Şebnem HARSA
Department of Food Engineering

[signature]
....   29.09.99
Prof. Dr. Muhsin ÇİFTÇİOĞLU
Head of Interdisciplinary
Material Science and Engineering Program

ACKNOWLEDGMENT

ABSTRACT

Nanocrystalline Titania was prepared by a chemical synthesis technique commonly known as sol-gel method. In the sol gel method, Titanium (IV) Isopropoxide was mixed with Isopropanol and Nitric Acid solution in predetermined ratios. A rapid hydrolysis reaction occurs between Titanium (IV) Isopropoxide and water in the Nitric Acid solution resulting in the formation of Titan oxide (Titania). The sols were clear sols and then gelled without any change in its clarity.

Nanocrystalline Titania were tried to prepare by two different techniques in this work. The first technique involved the drying of the gel and subsequent sintering of the dried gel. A number of organic additives (oxalic acid, acetic acid, polyacrylic acid and stearic acid) were mixed into the sol before gelation in order to control drying (drying control chemical addives-DCCAs). Powders was prepared from sols and gels by several processes and a solid form was obtained by dry pressing and subsequently sintered in second technique. Oxalic acid was the most efficient DCCA among the others.

The dried gels and powder compacts were sintered at 650, 700, 750, 800, and 850°C. The sintering behaviors of them were examined. Relative densities of the dried gels were between 79-99% depending on the sintering temperature. The green body density of the pellets were varied between 41-52%. Their relative densities after sintering were varied between 55-83% depending on the sintering temperature. The pellets were pressed at different pressures to observe the pressure effect on the densification. Increase in pressure improve the densification behavior. The best route for the nanocrystalline powder preparation was the Route 4. This powder had smaller size of agglomerate most probably the agglomerates were broken during the ultrasonic radiation.

The pore size analyses showed the pore structure of the gel. The pore size of the gels are about 35 nm. FTIR Spectra gave the crystal structure of the sols gels and powders.

As a result, the sintering behavior of the dried gels is better than the powder compacts. The pellets can be densified to higher densities by appropriate forming technique. Although, the dried gels have significantly high densities, the shape and the weight of the gels can not be controlled.

ÖZ

Nanoboyutlu Titanyumoksit sol-gel olarak bilinen kimyasal sentezleme yöntemiyle hazırlanmıştır. Titanium (IV) Isopropan alkol, Isopropan alkol ve nitrik asit çözeltisi ile hesaplanmış oranlarda karıştırılır. Titanium (IV) Isopropan alkol ve nitrik asit çözeltisindeki su ile Titaniyum oksit oluşturan hızlı bir hidroliz reaksiyonu gerçekleşir.

Nanokristal titanyum oksit iki farklı teknik ile hazırlanmaya çalışıldı. İlk teknik jelin kurutulması ve arkasından sinterlenmesini içermektedir. Bazı kurutma kontrol kimyasal katkı maddeleri kurutmayı kontrol etmek amacıyla sol ile karıştırıldı. İkinci teknikte, sollardan ve jellerden bazı prosesler uygulanarak tozlar hazırlandı ve kuru presleme ile şekillendirilip sinterlendi.

Kurutulmuş jeller ve kompaktlar, 650, 700, 750, 800, 850°C'de sinterlendi. Sinterlenme davranışları gözlendi. Kurutulmuş jellerin relatif özgül ağılıkları 79–99% arasındaydı. Peletlerin sinterlenmeden önceki relatif özgül ağılıkları 41-52 arasında değişti. Sinterlendikten sonra sinterleme sıcaklığına bağlı olarak 55-83% arasında değişti. Peletler basıncın densifikasyon üzerindeki etkisini gözlemlemek için farklı basınçlarda preslendi. Basıncın yükselmesi densifikasyon davranışını geliştirdi.

Sonuç olarak kurutulmuş jellerin sinterleme davranışı peletlerinkinden daha iyidir. Peletler daha yüksek özgül ağırlıklara daha iyi bir şekillendirme tekniği ile ulaşabilir. Kurutulmuş jeller pelletlere göre daha yüksek özgül ağırlıklara ulaşsada, şekil ve ağırlıkları kontrol edilemedi.

TABLE OF CONTENTS

LIST OF FIGURES

LIST OF TABLES

Chapter I

INTRODUCTION

The history of ceramic processing covers a long time span. Ceramic processing involves a great variety of processes like simple processes developed in ancient times for natural materials to the relatively sophisticated processes dependent on synthetic materials that are recently developed.

Traditionally ceramics had been made of inorganic, nonmetallic, rocklike materials. There are three general processes: [17] heating a raw material to prepare a cementitious powder that can be shaped by hand mixing and set to form a permanent product by hand building, [19] shaping a powder and then heating it to form a permanent product, and [45] melting a glass that is cooled to form a permanent product [17]. All these processes date back to before 5000 BC. The first forming machine was probably the potter's wheel, which was used earlier than 3500 BC. Shaping by pressing material in fired molds and firing in a closed kiln were subsequent developments.

The most remarkable achievement in 18th century was the development of pure white porcelain of high translucency in China. In 1708, F. Bottger and C. von Tschirnhaus (german alchemist and physicist) [19] found that fine porcelain could be produced on firing a body containing a fire resistant clay with fusible materials.

The introduction of steam power in the 19th century led to the mechanization of mixing, filter pressing, dry pressing, and pebble mill-grinding [17]. These developments accelerated the advances in ceramic powder technology. Significant advances in basic sciences including chemistry made it possible to synthesize new compounds. Metal alkoxides were prepared and studies on polymerization of alcohols and acids in solutions were done to form higher-molecular weight sols. Sol-gel transformation was studied.

In the first half of the 20th century, rapid developments in x-ray techniques for the analysis of the atomic structure of crystals were developed. Electron microscopy for examining the microstructure of materials was invented later. Material became more refined, and special compounds were developed, synthesized, and fabricated. Refined organic additives were introduced to improve the processing behavior.

In the second half of the 20th century, major advances in the synthesis, characterization, and fabrication of ceramic products has been improved. Scanning electron microscopy is now used for microstructural analysis and also several different instrumental techniques have been developed for bulk chemical analysis at very low concentrations and surface concentrations a few atomic layers in thickness [19].

These rapid developments in technology in the last couple of decades made it possible to synthesize a new generation of ceramic materials known as high technology ceramics (also known as advanced ceramics or fine/ultra-fine ceramics). A closer observation and control over the composition and microstructure of these materials resulted in superior material properties. These materials are prepared by different methods which have been recently developed. This new generation of ceramics fulfill special mechanical, chemical, thermal and electrical requirements no other material can satisfy.

Ceramics are mostly polycrystalline materials and they are composed of grains. Advances in the last couple of dedaces made it possible to produce ceramics having grain sizes in the sub-micrometer (0.1-1 m) and nanosize (1-100 nm) range. The reduction in the grain size was accomplished by using a number of recently developed powder synthesis methods. The grain size has important effects on the properties. The preparation of ceramic materials with nanosized grains, commonly known as nanocrystalline ceramics, will have significant effect on the current potential applications of advanced ceramics.

In this work, the preparation of nanocrystalline ceramics by using sol-gel techniques have been investigated. Clear sols of Titania prepared by using titanium alkoxides were gelled by aging at room temperature. These gels containing drying control additives were further dried to form dense compacts with nanometer sized particles. The sintering behaviors of these dried gels were examined. Powder was also prepared from these dried gels and similar characterizations were performed initially compacted pellets.

Chapter II

NANOCRYSTALLINE CERAMICS

Helbert Gleiter used a simple vapor deposition method to produce a metal powder by condensation from a metal vapor in 1984. The produced metal particles about 5-20 nm in size was compacted and then sintered to form a solid which was composed largely of grain sizes in nanoscale. This material showed amazing properties, for example, a 1000% increase in fracture stress (Fe-1,8%C), a 2000% increase in magnetic susceptibility (Sb) and an 80% increase in thermal expansion coefficient (Cu). Although some of these properties were disputed immediately, the following reports verified a new form of matter which was also called as nanophase or nanocrystalline material [30].

It is not long before that nanocrstalline ceramic powders were also produced by similar gas phase techniques. These powders were produced by subsequent oxidation of the metal vapors in gas phase or by direct vaporation and condensation of ceramics with high vapor pressures like ZnO, Mgo etc. Thus, the era of nanocrystalline ceramics had began. These amounts of powders produced through these gas phase techniques areso small hat researchers are trying to devlop new methods for the bulk preparation of these nanocrystlline ceramic powders [34].

Nanocrystalline ceramics are materials possessing grain sizes lower than 100 nm. For example a nanometer is a billionth of a meter and an average size of an atom is on the order of 1-2 A° (0.1-0.2 nm) in radii. Commercial ceramics have usually grain sizes bigger than micron or higher. The number sizes and the numbers of grains per unit volume are very significantly different in commercial and nanocrystalline ceramics directly affecting the materials properties.

2.1. The Reasons behind the Recent Interest in Nanocrystalline Ceramics

The motivation of studying and producing nanocrystalline ceramics lies in the unique chemical, physical and mechanical properties they possess. As the grain size gets smaller and smaller, larger and larger fraction of atoms resides on the grain boundaries.

Thus the behavior of a nanocrystalline ceramic is often controlled by events at the grain boundaries. For example, nanocrystalline ceramics can deform plastically and extensively by grain boundary sliding at moderate temperatures. This behavior is known as superplastic deformation that is in sharp contrast to the usual brittle behavior associated with commercial ceramics. Because of their presence of a large number of grain boundaries per unit volume near-net shaped pieces can be produced without any machining processes These materials have very low cracks and defects. The great number of the grain boundaries also cause many short circuit diffusion paths, so nanocrystalline ceramics could be used as a solid state bonding agent to join materials [35].

They are also indications that nanocrystalline ceramics have extremely low thermal conductivity. Thermal conductivity is directly proportional to the mean path length of phonons which is delimited by phonon-phonon scattering events. This is the order of a few nanometers in nanocrystalline ceramics. The distance between grain boundaries approach to the nanometer scale and hence the grain boundaries can also contribute to the scattering processes. If this process is realized commercially, nanocrystalline ceramics could become a valuable thermal barrier coating materials.

Nanocrystalline ceramics are sintered at lower temperatures. Staring materials with nanoscale particle sizes are used for the production of nanocrystalline ceramics hence the sintering process is completed at lower temperatures than the commercial ceramics that have considerably bigger particles.

All these properties give an opportunity to get lower cost and energy consumption during preparation of nanocrystalline ceramics with valuable properties than commercial ceramics.

2.2. General Properties of Nanocrystalline Ceramics

Nanocrystalline ceramics have superior physical, chemical and mechanical properties. Their smaller grain sizes, extremely large grain amount of boundaries per unit volume, and the opportunity of producing fully dense ceramics results in extremely useful properties such as being hard, strong, wear-resistant, corrosion-resistant, erosion-resistant and superplastic. Nanocrystalline ceramics are also sintered at extremely low temperatures.

Ceramics are brittle at low temperatures, but if they have grain sizes fine enough (about 15-20 nm), they become superplastic at moderate temperatures. Nanocrystalline ceramics have extremely high number of small grains which make them superplastic. Superplasticity is the ability of the polycrystalline material to experience large elongations to failure at moderate temperatures. Individual grains in the material are able to slide past each other during deformation. But unfortunately the strain rates of nanocrystalline ceramics are very slow. The deformation operation may take hours or even weeks. In order to increase the strain rate, the grain sizes must be reduced. The equation of superplastic flow is

$$\dot{\varepsilon} = \frac{A}{kT} \left(\frac{b}{d} \right)^{p} \left(\frac{\sigma}{E} \right)^{n} D_{o} \exp\left(-\frac{Q}{kT} \right) \qquad \text{(Eq.2.1)}$$

In this equation, A is a material constant, k is Boltzman's constant, b is their Burgers vector, d is the grain size, p is the grain size exponent, σ is the applied stress, E is young's modulus, n is the stress exponent, Do is the pre-exponential factor for diffusion, Q is the activation energy for superplastic flow (presumably $Q_{superplastic} = Q_{diffusion}$), and T is the temperature in degrees Kelvin. Of importance here the fact that p often takes on values of 2-3, so that for a factor ten decrease in grain size, it could be obtained that the factor of 1000 increase in forming rate. These faster rates represent the motivation for attempting to fabricate and test ceramics with nanocrystalline grain sizes [36].

The first indications to this behavior were observed by Karch, Birringer and Gleiter [16]. These researchers demonstrated that nanocrystalline TiO_2 and nanocrystalline CaF_2 films would deform a moderate amount, at room temperature, under combined compression and bending stress. Later experiments showed that nanocrystalline TiO_2 ceramics did not crack under small loads, whereas a single crystal or large-grained polycrystal did. The experiments were done on TiO_2 at elevated temperatures by Hahn at al. [15]. At 800°C, roughly 0.5 of the melting point of TiO_2, compressive strains about 60% at a strain rate of $1.1. 10^{-5}$ s^{-1} were obtained, and subsequent tests showed that nanocrystalline ceramics could deform at a strain rate of up to 1 s^{-1} with a characteristic stress exponent of $n \cong 3$.

Nanocrystalline ZrO_2-3mol%Y_2O_3 (about 80 nm grain size, see Figure 2.1) produced by a chemical precipitation technique and commercial powder (0.3 µm grain size) at the same composition were tested at 1150°C. The results showed that the rate of

deformation of nanocrystalline ZrO_2-3mol%Y_2O_3 was approximately 34 times faster than that of the commercial one [16]. The strain rates are shown in Figure 2.2.
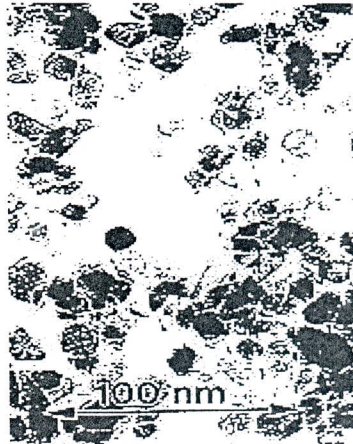
Figure 2.1. Nanocrystalline starting powder used in fabricating yttria stabilized Zirconia compression specimen. [36]
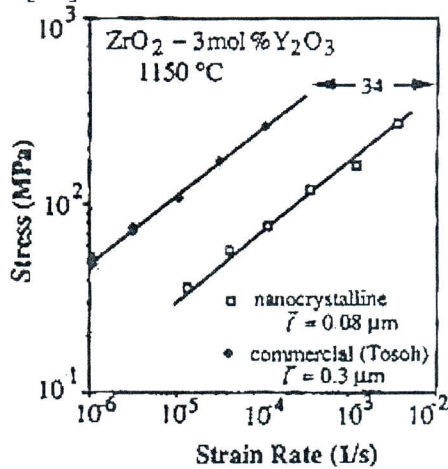
Figure 2.2. Stress-strain rate relationships for fine-grained and nanocrystalline ZrO_2-3mol%Y_2O_3. Data from compression tests conducted at constant crosshead speed. [36]

The following Figures (Figure s 2.3-2.4) show the superplastic behavior of nanocrystalline ZrO_2-3mol %Y_2O_3.
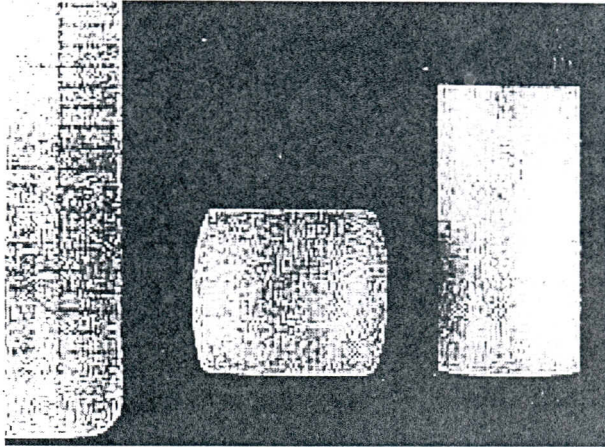
Figure 2.3. Superplastic ZrO_2-3mol %Y_2O_3 fabricated from Tosoh TZ-3Y powders. Samples before (left) and after (right) compressive deformation at 1150°C[35].
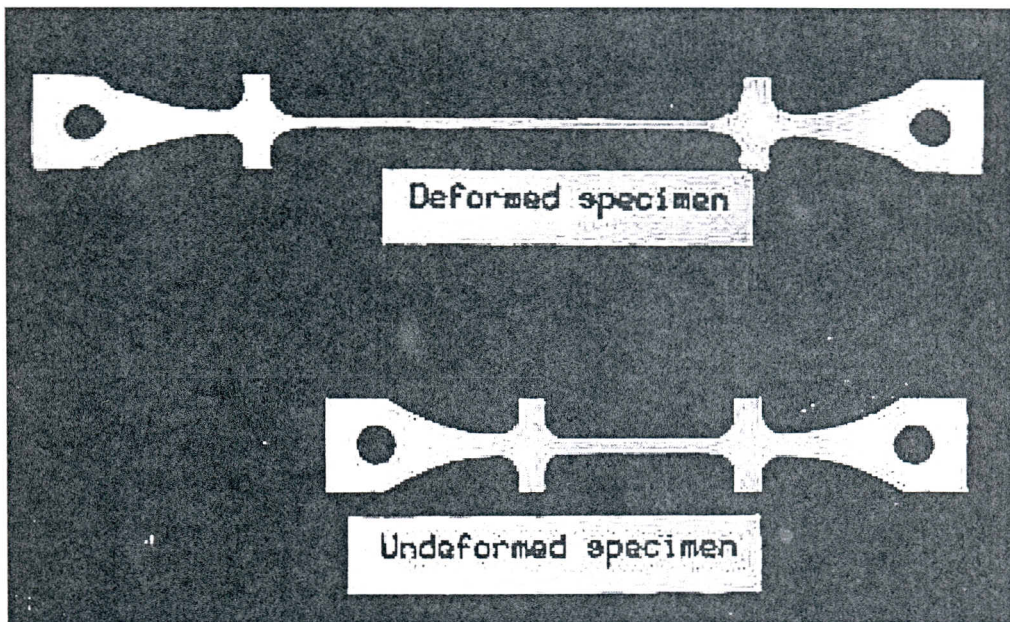
Figure 2.4. Superplastically elongated specmen of Y-TZP at 1450°C·

Nanocrystalline ceramics have an opportunity to be sintered at lower temperatures than that of commercial ceramics. Reducing the starting particle size to 13 nm allowed ZrO_2-3mol %Y_2O_3 to be presurreless sintered to nearly full density at 1050°C as shown in Figure 2.5.
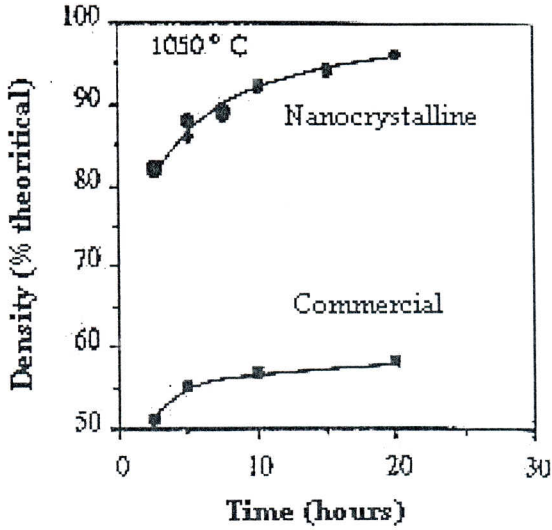
Figure 2.5. Density of nanocrystalline vs. commercial (Tosoh T-3Y brand) ZrO_2-3mol %Y_2O_3 as a function of holding time when isothermally sintered at 1050C (5°C/min. heating rate). Starting green density =44% [15].
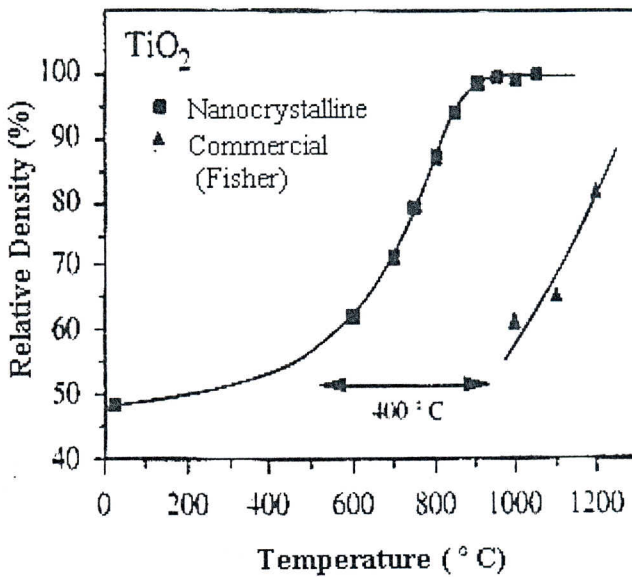
Figure 2.6. Sintering behavior of nanocrystalline and commercial Titania [35].

The sintering behavior of nanocrystalline ZrO_2-3mol %Y_2O_3 at 1050°C is significantly better than that of commercial ZrO_2-3mol %Y_2O_3 (Figure 2.5.). The sintering temperature of nanocrystalline Titania (Figure 2.6) is about 400 lower than that of commercial Titania.

2.3. Present And Potential Applications of Nanocrystalline Ceramics and Materials

Nanocrystalline ceramics are currently in use and have also a wide variety of potential applications. Nanocrystalline ceramics can be used as highly sensitive sensors. Sensors employ their sensitivity to the changes in various parameters they are designed to measure. The measured parameters are generally electrical sensitivity, chemical activity, magnetic permeability, and thermal conductivity. The measurements of all these parameters greatly depend on the microstructure of the sensor material. Nanocrystalline ceramics can measure these desired parameters very sensitively because diffusion occurs along grain boundaries. Grain boundary diffusion is as much as 1000 times faster than lattice diffusion. For example, oxygen ions move through grain boundary path. Thus, nanocrystalline ceramics can be used as highly sensitive sensors, which are capable of operating at much lower temperatures than the systems currently in use today.

Nanocrystalline ceramics can be described as deformable ceramics because of their superplastic behavior. Superplasticity presents a real possibility that near-net-shaped pieces can be produced directly from solid stock nanocrystalline pieces by common metal-forming techniques. From the phenomenological equation (see eq.2.1) for superplasticity, decreasing the grain size can significantly improve the strain rate. Smaller and smaller the grain size gets, faster and faster the strain rate becomes. Ceramics must have 15-20 nm grain size for an ideal superplastic deformation. Hence, the ceramics would deform at strain rates and temperatures currently used today for superplastic metal forming operations.

The low sintering temperatures will allow ceramics to be co-processed with metals in a variety of applications. In multicomponent materials the use of nanocrystalline ceramics can significantly reduce the thermal mismatch stresses generated during component fabrication. Nanocrystalline ceramics are also capable of exhibiting stress

relaxation (through superplastic flow) which would tend to reduce the residual thermal stresses.

They can also have a potential application of diffusion bonding for gluing larger ceramic parts. Sinterability at low temperatures make this operation possible at lower temperatures. Molten-glass, reactive braze metals, and epoxies have been used with some success as high-tech adhesives. However, they don't retain their strength at elevated temperatures [35]. At these temperatures nanocrystalline ceramics retain enough strength. With enough pressure and temperature, two clean ceramic components can be mated and bonded to form an invisible, seamless joint. This operation could be made at lower temperatures, which is in contrast to the conventional ceramics. There are three advantages of using nanocrystalline ceramics for bonding applications. First one is the high diffusivity in nanocrystalline material that accelerates transport of matter across the joint. Secondly, superplastic nanocrystalline ceramics can flow plastically to conform to the contours of a microscopically rough surface. Thirdly, nanocrystalline ceramics used as an interlayer between two layers with larger grains hence the difference between grain sizes encourage the grain growth across the interface. As a result, the joint materials and the parts mechanically lock and chemically bond to each other as shown in Figure 2.7
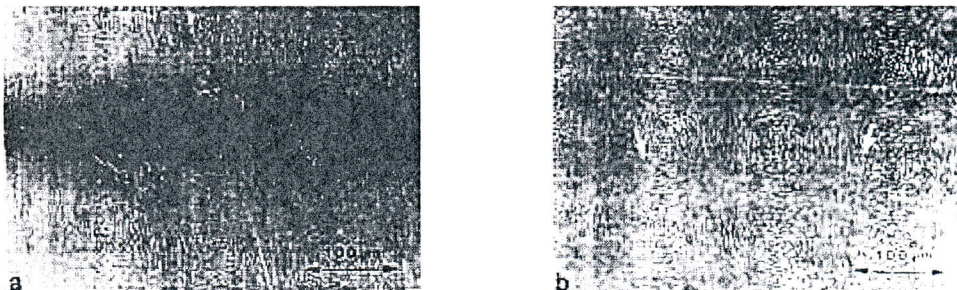
Figure 2.7.Joining of ZrO_2-3mol %Y_2O_3 ceramics. – A direct diffusion-bonded joint between two commercial ceramics (grain sizes are about 450 nm) at 1090°C and 10 MPa of pressure. B- A joint between two nearly-nanocrystalline ceramics (grain sizes are about 180 nm) fabricated under the same conditions. Both samples were etched with ammonium floride to bring out the joint line [35].

Nanocrystalline ceramics have small size and very narrow distribution of pores so that it is possible to use them as filters that are very selective (to within 1-3 nm) in the 5-20 nm range. These filters have also an advantage to be produced by using standard pressing and sintering procedures.

Nanocrystalline ceramics are currently in use because of their erosion and corrosion resistances. Aerospace and automobile components are coated with nanocrystalline ceramics. Since nanocrystalline ceramics are non-porous, hard, wear resistant, biocompatible, unreactive with human tissue and have lightweight, nanocrystalline ceramics can be used as implants (as a main material or coating material).

In summary, generally nanocrystalline materials have a wide variety of applications present and potential applications. They may have many other and applications based on a number of functions such as electrical and magnetic functions (as insulation, ferroelectrics, piezoelectric, semiconductor ion conducting materials), optical functions, chemical functions (as gas, humidity, catalyst carrier, organic catalyst, electrodes), thermal functions (as an infrared radiator), mechanical functions (as cutting tools, wear-resistant material, heat resistant material) and biological functions (as implantation, hydroxyapatite bioglass).

Chapter III

SYNTHESIS OF FINE CERAMICS

Fine ceramics are produced mostly from powders through mainly two different routes that are conventional and non-conventional routes. Controlling the particle size and particle size distribution of the powder has a great importance in achieving optimum properties of the final ceramic.

Ceramic powder processes can be divided into two parts as conventional and non-conventional powder preparation techniques. Conventional techniques are largely used in ceramic industry that involve the normal mixing, calcining, and grinding operations. Non–conventional techniques are also used for the production of ceramics widely but they aren't comprised of the operation mentioned above [9].

Table 3.1 Powder Preparation Techniques [37].

Size reduction techniques	Screening Elutriation Air Classification Sedimentation Ball milling Attrition Milling Vibratory Milling Fluid Energy Milling
Chemical synthesis techniques	Precipitation Sol-Gel Liquid Mix Decomposition Freeze drying Hot kerosene Drying Hyrothermal Plasma
Miscellaneous techniques	Calcining Rotary Kiln Fluidized Bed Combustion Synthesis

Size reduction involves several techniques that are based on reduction of the size of the particles by mechanical means. In screening is the powder is poured onto a series of screens, each subsequently with smaller holes from the top to the bottom. The particles are separated into size ranges; particles larger than the screen remain on the screen and smaller particles pass through the screens until they reach a screen with the holes too small to pass through. Screening process can be conducted dry or wet. Dry screening is used mostly for larger particles, for example in mining industries. The particle sizes that are below 325 mesh is referred as fine particles tend to agglomerate and behave as a single particle. Thus, inaccurate screening occurs. Screening of a suspension, wet screening, aids to disperse these fine particles in a liquid -mostly water- so that the fine particles are able to pass through the screens without any agglomeration and dust problems.

Air classification is used to separate fine particles from coarser fractions of dry powders. Separation is achieved by controlling the horizontal centrifugal force and vertical air currents within the classifier. Particles enter the air classifier along the center line. While the coarse particles move radially away from the central separating zone to a collection cone, the fine particles are carried upward and move by the air currents through the selector blades. A basic air classifier is shown in Figure 3.1. Air classification method for fine particles below 10 µm is not sufficient.

Sedimentation technique is based on particle separation according to the settling rates of particles suspended in a liquid. The larger particles settle down more rapidly than the fine particles so that the upper part of the suspension is separated and the remaining liquid is removed. The main problem would be agglomeration of the particles during the liquid removal similar to the wet screening separation technique.

Ball milling is used when screening, air classification and sedimentation are not enough for the preparation of fine powders in bulk quantities. The first three techniques are mainly separation techniques but ball milling is one of the most widely used size reduction techniques. Ball milling consists of placing particles to be ground in a closed cylindrical container as a grinding medium and rotating the cylinder horizontally as shown in Figure 3.2. The powder particles are efficiently broken into smaller particles while they move between the media and the wall of the mill. Relative size, specific gravity and hardness of media and particles determine the rate of milling. The use of zirconia spheres as a grinding

media, and water as the vehicle, can be used to achieve a fast and more efficient milling process.

Attrition milling is very similar to ball milling. An attrition mill is cylindrical as a ball mill it does not rotate. The very small balls are agitated by a series of stirring arms mounted to an axial shaft as shown in Figure 3.3. This technique is more efficient than the ball milling.

Vibratory milling is substantially different from ball milling or attrition milling. Powder is placed in a stationary chamber of the mill with a suitable grinding media and a liquid. When mill is turned on vibration is transmitted (usually from the bottom of the centre of the mill. This results in two different movements. The first one causes a mixing action of the powder and the second one causes a local impact and shear fracturing of powder particles between the adjacent grinding media.

Fluid energy milling technique is achieved by particle-particle impact in a high-velocity fluid. The fluid can be a compressed gas or liquid compatible to the equipment design. The powder is added to the compressed fluid and accelerated to sonic or near-sonic velocity through the grinding chamber. The grinding chamber is designed in order to minimize the particle-particle impacts and minimize particle-wall impacts.

Finer particles can be obtained by using chemical synthesis techniques. High purity powders are produced with well-controlled particle size by these techniques. A typical chemical synthesis technique involves three major steps: the preparation of the precursor, the removal of the solvent, and the conversion of the precursor to the desired product. Precipitation technique is one of them. Generally, a metal salt which is acidic is added into a basic medium. The introduction of highly acidic solutions into highly basic solutions result in the precipitation of the hydroxides. This process is influenced by several factors like the temperature, concentration, pH, rate of mixing, and washing. After the removal of the solvent, calcination process is get the final powder.

Freeze-drying is another chemical synthesis technique that has a potential to produce uniform particles and crystallite sizes with high homogeneity. There are four basic steps in freeze drying process. A mixture of desired amount of metals is dissolved in water. The solution is rapidly frozen and the water is removed under vacuum by sublimation. The precursor powder is calcined finally.
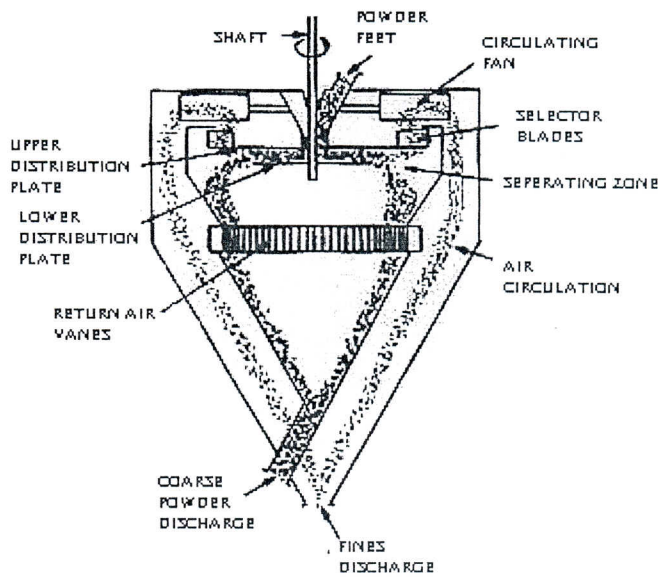
Figure 3.1. A schematic illustration of an air classifier showing the paths of the coarse and fine particles [37].
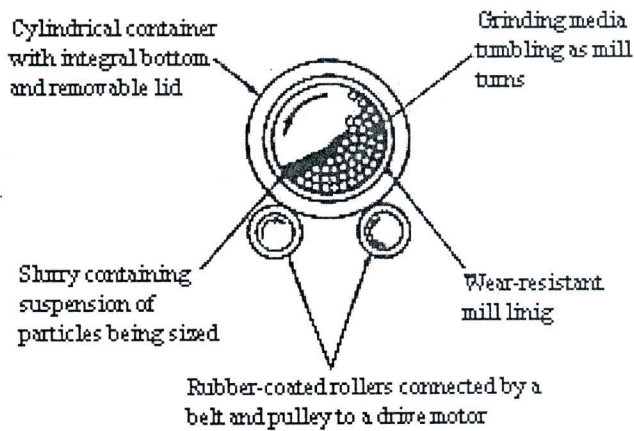
Figure 3.2. Schematic illustration of a typical ball mill cross-section showing the key elements [37].
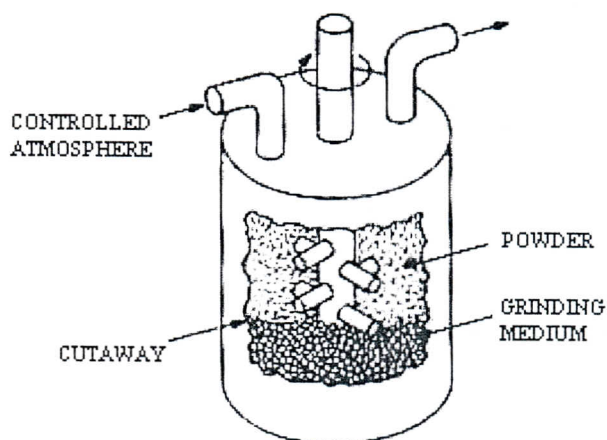
Figure 3.3. A schematic illustration of attrition milling [37].

Hot kerosene drying is an alternative to freeze-drying for the salts that can not be processed by freeze-drying. The water-soluble compounds at desired amounts are mixed with water and then vigorously mixed with hot kerosene (at 170°C) with an emulsifying agent to form an emulsion. During mixing, water is evaporated rapidly and the remaining salts are separated from kerosene by screening. The salts are thermally decomposed in air to form the oxide. This method can be performed by other organic fluids.

Sol-gel is a widely used ceramic processing method. Compositions high purity can be achieved at molecular level synthesis at large quantities. The basic steps of the process are the formation of a sol in a liquid, gelation of the sol by evaporation of the solvent, addition of an electrolyte or aging, and evaporation of remaining solvent from the gel. Finally, thermal treatment of the gel or the powder compact produced from the gel is performed. This method is described in detail in Chapter IV.

Hydrothermal synthesis involves crystallization of a powder in hot and pressurized water (for example, water temperature is about 100-350 °C and pressure up to 15 MPa). A wide variety of pure and fine ceramic powders can be synthesized by this method. The resulting powder consists of single crystals and no heat treatment and milling processes are required. This synthesis technique has been performed in laboratory scale not scaled up to commercial production.

Miscellaneous powder synthesis techniques involve calcining, rotary kiln, fluidized bed and self-propagating combustion techniques. Calcining refers to a high temperature treatment of a powder to modify the characteristics of the powder. Coarsening, decomposition and dehydration are most common modifications that calcining can achieve. Coarsening involves crystallite growth or fusing or bonding small particles together to produce larger particles. Decomposition method involves converting compositions such as carbonates and nitrates to oxides. Dehydration is important in preparation of hydraulic cements and plaster [37].

Gas condensation technique produces nanometer-sized powders. The system consists of an ultra high vacuum system, heated evaporation sources, a liquid nitrogen-filled condensation tube, and a scraper to remove condensed powder from the surface of the tube.

3.1. Powder Characterization

The physical and chemical characteristics of ceramic powders strongly influence the behavior during further processing and the performance of ceramics. Detailed information on powder characteristics is required to achieve adequate control of large-scale production of fine ceramics. For example, sintering depends on the reduction of surface area of the powder thus, the surface area of the powder must be determined for understanding the sintering behavior of the ceramic.

Particle size distribution, particle morphology, surface area, and state of agglomeration are the most important physical properties of a ceramic powder. How well a powder can be packed during green body formation greatly depends on these properties. Powders containing hard agglomerates are undesirable because those do not break down during green body formation. Therefore, they can lead to differential sintering that result in non-uniform microstructures and reduced densities. There are many techniques for determining physical properties of powders. These techniques use sizing techniques that are based on a variety of principles, including sedimentation, light scattering, electrical sensing, image analysis of electron photomicrographs, hydrodynamic chromatography, and sieving. X-ray diffraction line broadening that is often used to determine a powder's average crystallite size and is applicable when crystallite sizes are less than 1000 A°.

Particle morphology is characterized by image analysis of photomicrographs obtained using scanning electron microscopy (SEM) or transmission electron microscopy (TEM).The most widely used method to determine the specific surface area of a powder is by the application of the Brunauer-Emmett-Teller (BET) model to gas adsorption data. Agglomerate strength can be inferred from powder compaction data. A technique developed by Ciftcioglu and co-workers combines particle size distribution analysis with ultrasonic disruption to determine agglomerate strength [43]. In this method, powder suspensions are subjected to ultrasonic radiation with an intensity that has been calibrated in terms of disruptive pressure. Particle size distribution data are measured after fixed times at progressively higher power inputs. The change in particle size distribution as a function of sonication intensity and time is related to agglomerate strength [43].

Chemical properties can be determined by thermal analyses that are often used to characterize the decomposition and crystallization behavior of ceramic precursor powders. The information gained from this kind of analysis is used to determine appropriate calcination schedules. The most common thermal analysis techniques are thermal gravimetric analysis (TGA), in which weight loss is measured during heating, and differential thermal analysis (DTA), in which the changes in temperature of the sample relative to a standard are measured during heating.

Chapter IV

SOL-GEL PROCESS

Sol-gel is a chemical process of preparing ceramics, glasses and glass-ceramics. It involves chemical synthesis of hydrolyzable alkoxides and metal salts which can undergo a sol-gel transition.

Sol is a colloidal suspension of solid particles in a liquid. The dispersed phase is so small in size (~1-100 nm) that the gravitational forces are negligible. The interactions between particles, however, are dominated by short range forces such as van der Waals forces and surface charges. Three-dimensional network of the dispersed solid particles is called gel. It differs from a sol for being resistant to shearing forces.

Sol-gel process may be used in ceramic and glass-ceramics material processing with two different routes as shown schematically in Figure 4.1. These are powder and powder-free routes. In powder route, discrete particles are processed in order to form bulk component. Starting from hydrolyzable alkoxides, powder-free route generates a porous preform of a glass or a ceramic by linking molecular species. Depending on composition, precursor, handling, and heat treatment[1] the final structure is either amorphous or crystalline.
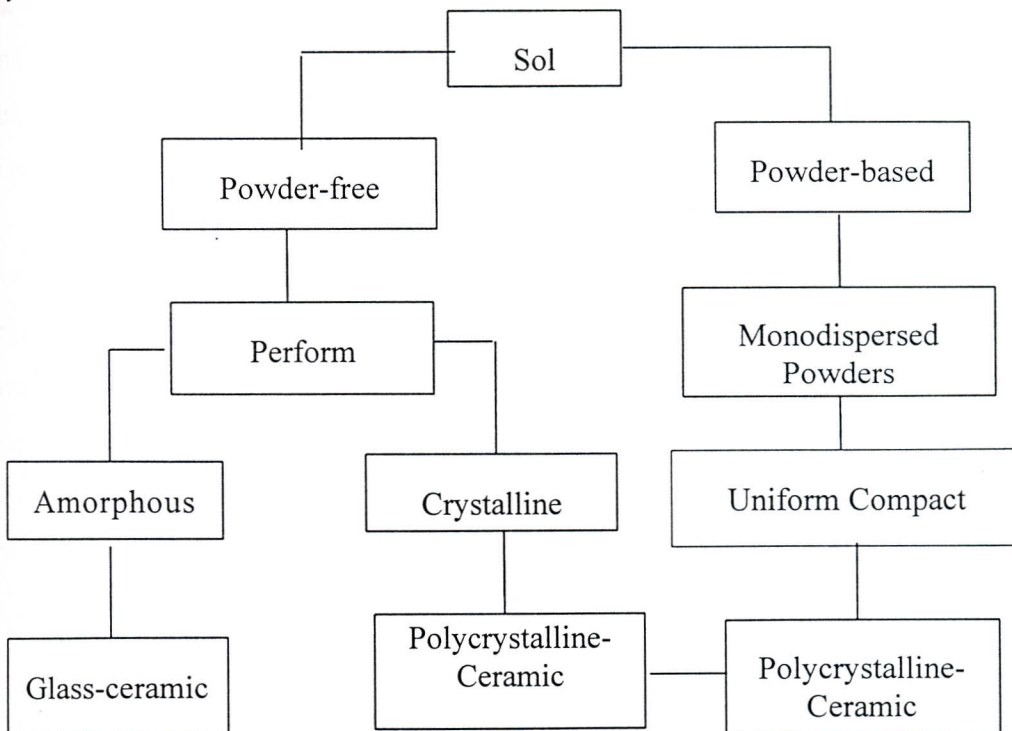
Figure 4.1. Preparation of glass, glass-ceramics, and ceramics by the sol-gel method.

4.1. Sol-Gel Chemistry

The first step of the sol-gel process is the preparation of the sol starting from either a metal salt aqueous solution or a metal alkoxide organic solution i.e. by using titanium isopropoxide. This step is followed by the hydrolysis reactions. Hydrolysis reactions can be accomplished either by changing the pH in metal salt solutions or by adding water to alkoxide solutions. Water addition to alkoxide solution forms reactive M-OH groups which upon condensation form metal-oxygen-metal bonds and condensed species, colloids, gels and/or precipitates.

Hydrolysis-condensation processes may be represented by following reactions

$$M(OR)_4 + H_2O \rightarrow M(OR)_3(OH) + R(OH)$$ *Hydrolysis Reaction*

$$M(OR)_4 + M(OR)_3(OH) \rightarrow M_2O(OR)_6 + R(OH)$$ *Condensation Reaction*
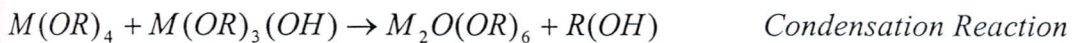
In these reactions M stands for a metal such as Si, Ti and Zr and R for organic group. These reactions can happen under acidic, basic or neutral conditions. The transition of sol to gel is called the gelation process. In this process, the sol losses its fluidity and takes the appearances of an elastic solid at a point generally called the gel point. The difference between sol and gel is shown in Figure 4.2. schematically. Transition at the gel point occurs with no volume change and is determined by inspecting a sharp increase in viscosity.

The gel formation stages in acid and base-catalyzed systems as shown Figure 4.3. Bonds between the stationary clusters are formed (particles in sol) near the gel point. The bond formation, however, continuous after the gel point. Gel formation step may be, however, accelerated by the addition of suitable chemicals such as H_2O_2 and/or evaporation of solvent [15]. In the first place, the network is initially compliant, still move close enough together to allow further condensation. Moreover, there is still a sol within the gel network and those particles continue to attach themselves to the network.
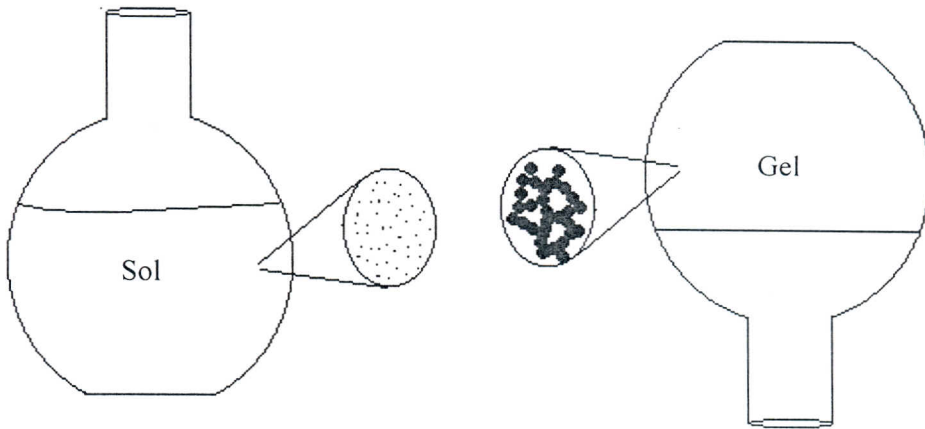
Figure 4.2. An illustration in the difference between a sol and a gel.
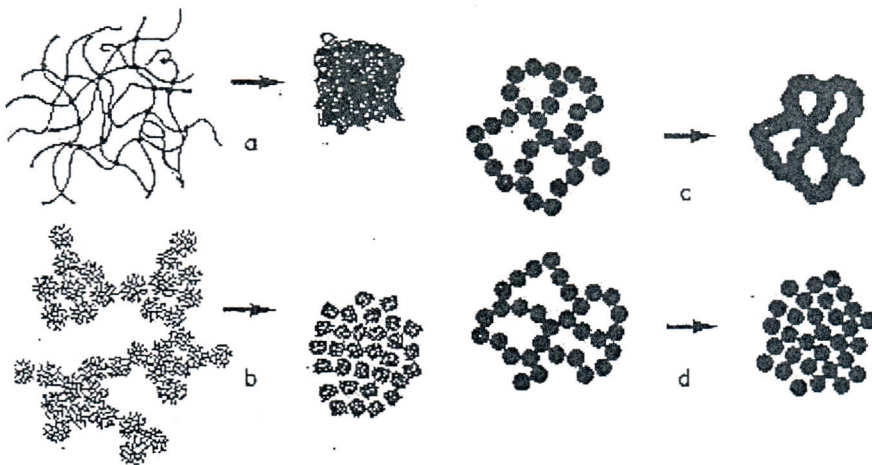
Figure 4.3. Schematic representation of gel desiccation for (a) acid-catalyzed, (b) base-catalyzed gels, (c) colloidal gel aged under conditions of high silica solubility, (d) colloidal gel composed of weakly bonded particles [12].

Structure and properties of a gel change in time. This is called aging. The processes occurring during aging are categorized as polymerization, syneresis, coarsening and phase transformation.

The increase in connectivity of the network produced by condensation reaction is called polymerization and for example is represented as

$$\equiv Si - OH + OH - Si \equiv \rightarrow \equiv Si - O - Si \equiv + H_2O$$
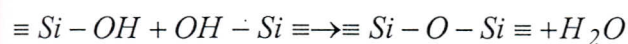
Polymerization strengthen the network by forming additional bridging bonds and its rate depends on several parameters including temperature and concentration and pH of the solution. Shrinkage of the gel network as results of expulsion of liquid from the pores is called syneresis. It occurs, for example, by following reactions [12]:

$$\equiv Ti - OH + HO - Ti \equiv \rightarrow \equiv Ti - O - Ti + H_2O$$

and

$$\equiv Ti - OR + HO - Ti \equiv \rightarrow \equiv Ti - O - Ti \equiv + ROH$$
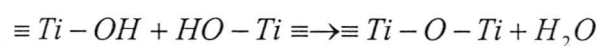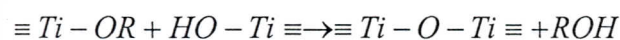
Dissolution and reprecipitation driven by differences in solubility is called coarsening or ripening. The dissolution of small particles followed by solute precipitation on large particles results in coarsening. Coarsening reduces the solid phase curvature and interfacial area and increases average pore size.

Several types of phase transformations can occur during aging. On a local scale, phase transformations separate solid phase from the liquid resulting in unreacted alkoxide in isolated regions.

The structural changes during aging have an important effect on the drying process. The capillary pressure that develops during drying is proportional to the interfacial area in the gel.

4.2. Drying Process

A gel is composed of two components: an oxide network and a solvent phase confined in pores. The solvent removal is accomplished by drying. The gel is similar to a porous media Drying process of the gel may involve several stages: constant rate period, critical point and first and second falling rate periods. These stages are schematically shown in Figure 4.4.

A) Initial Condition

liquid/vapor
meniscus

pore
liquid

solid
phase

B) Constant Rate Period

evaporation

shrinkage

C)First Falling Rate Period

empty pores

minimum
radius
curvature
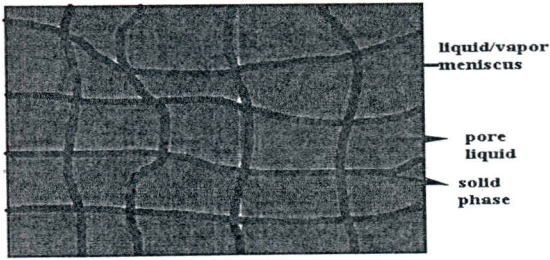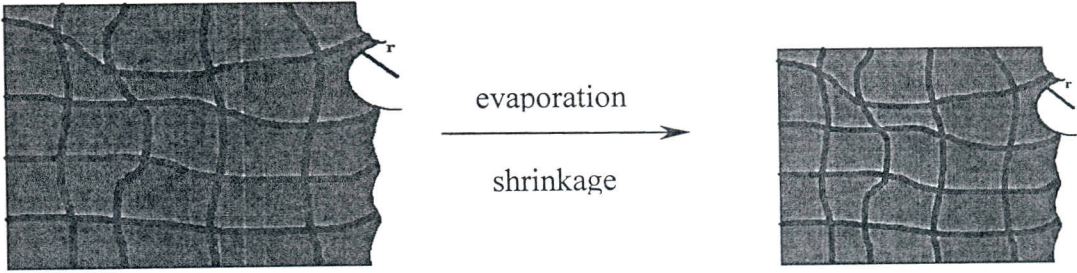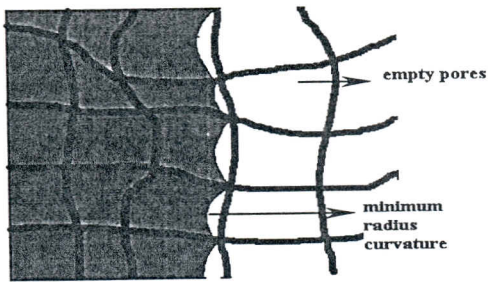
Maximum Capillary Pressure

$$P_R = \frac{(\gamma_{SV} - \gamma_{SL})S_P}{V_P}$$

D)Second Falling Rate Period

Diffusion

Flow
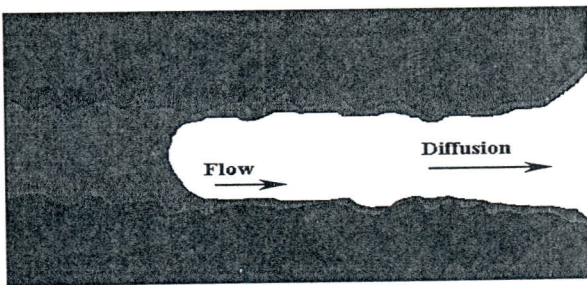
Figure 4.4. Schematic illustration of the stages of the drying process of the gel. a- before evaporation begins, the meniscus is flat, b- Capillary tension develops in liquid, c- During falling rate period, the liquid recedes into the gel, d- After critical point the liquid-vapor meniscus retreats in to the pores of the body. Flow of liquid and diffusion is possible in this stage [12].

The volume change in the gel is equal to the volume lost by solvent evaporation in constant rate period. In this stage, the solid network shinkages continuously as the solvent evaporates. Shrinkage stops at the end of the first stage. Gel tends to crack at this critical point. Liquid flow through partially empty pores in the first falling rate period. In the second falling rate period, the final stage of drying, liquid flows through the empty pores and evaporation of the liquid occurs via diffusion in two different ways: diffusion toward the outside in the very dry exterior region and diffusion toward the drying front from points within the partially drained pores.

The drying process of films can be achieved without any problem. Drying problems arise in the bulk samples known as monoliths. The monoliths tend to crack during shrinkage.

It is experimentally found that the plot of linear shrinkage versus time in drying of a gel monolith gives an S-shaped curve [5]. The shrinkage is initially as shown in Figure 4.5. The shrinkage accelerates to a linear rate. The evaporation rate at the surface equals to the diffusive flux to the surface in this linear rate region.
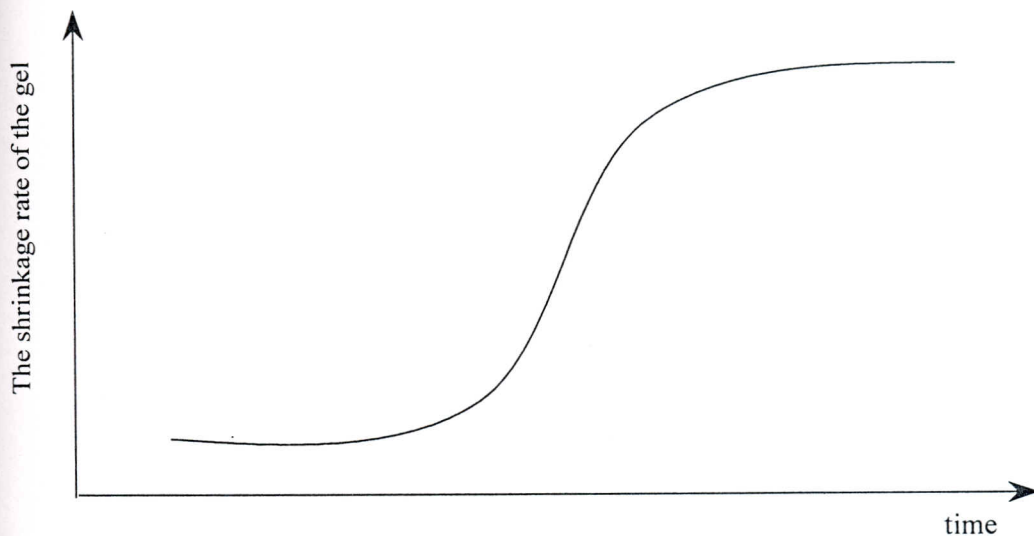
Figure 4.5. The shrinkage rate of the gel vs time.

As the network shinkages further, more hydroxyls are brought close together so that condensation increases. The dry fraction of the gel is larger than the wet fraction. Then

24

the question is whether or not strains in the materials are great enough to cause fracture at that point.

Defining an appropriate drying condition of a gel is difficult to achieve. One definition may be the time at which further weight loss is negligible. The time at which sample shows no adverse effect from ambient conditions may also be used as drying condition. Most of the gels, however, show a reabsorption of solvent; therefore, gel is not truly dry until after some stabilizing heat treatment.

Chapter V

FORMING PROCESSES

The objective of the forming process is to form a net-shaped, homogeneously dense powder compact that is nominally free of defects. Forming transforms any type of feed into "green product" has a controlled size and shape with a particular density and microstructure. Controlling over the density and the microstructure of the green body gives desired performance of the final product. Although the pores in the green body is eliminated by sintering, in order to study at lower sintering temperatures it is necessary to obtain higher density of in the green body by improving the forming processes. The most widely used forming processes are casting, extrusion, injection molding, and pressing (for further information see Reference 19).

Casting processes, which includes slip, tape, vacuum and pressure casting, are used to produce a self-supporting shape called a cast from specially formulated slurry. Slip casting utilizes a stable suspension of the ceramic body, normally in water or an organic solution with suitable additives for its rheology. The suspension is poured into a plaster mold. Water in suspension is then absorbed by the mold at its surface, resulting in the formation of a layer of material that is low enough in water content. After a layer of proper thickness has formed, the remaining slip is poured or drained from the mold. The part is normally allowed to remain in the mold for additional water removal, by mold absorption and evaporation, until the part has become physically strong enough to support itself. Finally, the mold taken apart to release the part, which is then dried. Tape casting is a specialized method of producing thin, flat and uniform strip that can be cut into various shapes. The thickness of the strip can be changed by solid content of the slurry, the speed of the carrier system and the drying shrinkage. It is also possible to get multilayer strips by this method. Vacuum casting is widely used for forming very porous refractory insulation having complex shape. Pressure casting is the direct derivative of slip casting, which is done by applying pressure on fluid, vacuum on mold. The mold serves as a filter and the casting time is controlled by external pressure. In some respects, gel casting is similar to slip casting. Both processes convert a type of slurry into a rigid cast part. Slip casting is an aqueous process, and gel-casting can be either aqueous or non-aqueous process. Slip

casting produces parts that are somewhat fragile and cannot easily be machined in the green state. Gel casting uses a high solids content of ceramic powders in an organic solvent. The solid loading is higher than that of slip casting. Gel cast parts are relatively strong and can be machined. However, the gel cast processes are less likely to have molding defects. These processes can produce thick-section parts, which is a problem with injection molding.

Extrusion is used to form ceramic bodies plasticized by organic binder(s). It involves shaping of the cohesive plastic material by forcing it trough a rigid die. Warm and cold extrusion can be performed by mixing sufficient amounts of binder and plasticizer materials to improve flow characteristics.

Injection molding is a well-known method of producing medium-sized complex shaped parts. In this process, the powder is mixed with suitable thermoplastic binder in a heated mixer. Then, the mixture is injected to the cooler mold under pressure by a piston or a screw system and then the mixture solidifies in it. After very short time, the green body can be removed from the die. In this process, the important parameters of the process are powder, organic binder, removal of organic binder, mold shape, mold material and temperature, and filling pressure and velocity.

Pressing is the simultaneous compaction and shaping of a powder or granular material confined in a rigid die or a flexible mold. The most known pressing processes are isostatic, hot, hot isostatic, die, and dry pressing. Isostatic pressing is done in flexible rubber molds, and also known as iso-pressing. It is used for producing shapes with relief in the shapes with one elongated dimension and very massive products with thick cross sections. Hot pressing is done at high temperature and basically combines pressing with firing. This process is limited by the die materials available and shapes can produced. Hot isostatic pressing is basically isostatic pressing at elevated temperatures. The pressure is applied from all sides as the part is held at elevated temperatures. Pressing by means of punches in hardened metal dies commonly is called as die pressing. It is generally used for pressing parts thicker than 0.5 mm and parts with surface relief in the pressing direction. Dry pressing, also known as compaction, differs from die pressing because of the moisture content. In die pressing the moisture content is about 10%, but in dry pressing it is below 4% and lubricant such as stearic acid or wax are used during dry pressing.

5.1. Compaction of Ceramic Powder

Powder compaction is a commonly technique. It involves with basic steps of a) filling the mold or die b) compacting the powder and c) ejecting the compact from the die. Pressing process is schematically shown in Figure 5.1.
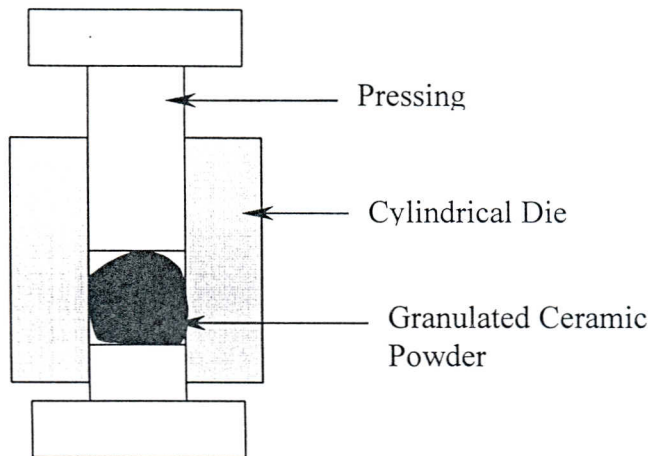
Figure 5.1 An illustration of pressing process.

Optimum pressing conditions are achieved by controlling several parameters carefully. These parameters are die-fill density, die-wall friction, expansion on ejection and packing density. Die filling affects directly the compaction density and also affects size, shape, and microstructure of the final sintered product. Another important effect is the uniformity and homogeneity of particle packing in the green body, which influenced the sintering behaviour of the green body.

Friction between the die and the powder decreases the pressure available for the compaction with increasing distance from the middle of the pressing punch. The friction results in density gradients in the compact. Smoothing the surface of the die may diminish frictional effects. Particle packing is the most important physical characteristic of powder compact. Particle packing density affects the sintering success and properties of the final product such as density, size and pores size distribution. Good packing density produces a finer and more uniform pore structure so that it can densify uniformly.

Various organic additives are generally added to the ceramic powder to ease the pressing operation and to enhance the compact properties. Binder(s) is added to improve strength, plasticizer(s) to increase deformablity, and lubricant(s) to reduce frictional

effects. When the purity of the final product is a primary concern, addition of these additives must be avoided.

Common defects observed in the final sintered product as shown in Figure 5.2. Very hard granules result in a low-density product and soft granules form side cracks due to density gradient. Defects formed due to density gradients can be classified as end capping, ring capping, laminations, and vertical cracks as they are shown in Figure 5.3.
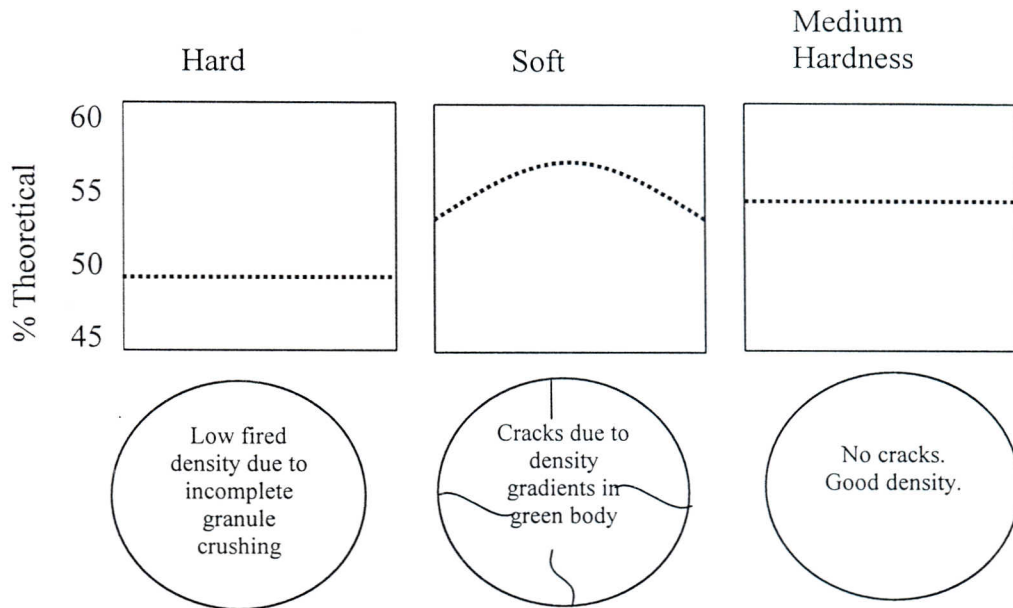
Figure 5.2 Qualitative results of Onoda's compaction experiments with nominally hard, soft, and medium hardness alumina granules compacted uniaxially using uneven die filling as illustrated in Figure 5.1[45].

Figure 5.3 Illustrations of typical end capping, ring capping, lamination, and vertical crack defects in cross-sections of cylindrical powder compacts pressed uni-axially from the top to down [45].

End capping is a central cone-shaped separation that forms at the pressing punch face. It is common in bodies having poor green body strength and at high pressing pressures. Ring capping is an outer-ring separation that forms at the outer edge of the pressing punch face. Laminations are periodic circumferential cracks in a compact that

29

originate the die surface perpendicular to the pressing direction. Vertical cracks are elongated cracks that form parallel to the pressing direction in the exterior region of a compact when there is an excessively high compaction ratio (compact density to die-fill density) [45].

Decades researches on conventional ceramic processing have shown that the uniformity and homogeneity of particle packing in the green body has a very important effect on how well the green body will densify during sintering as it is mentioned above. At this point nanocrystalline ceramic powder has some disadvantages. Because of their small particle size, the behavior of the powder is forming bonds between each particle in either dry or wet state. Even if no bond is formed during synthesis, the van der Waals attraction causes the powder particles to bond together into agglomerates during handling, drying or storage. The compaction of this agglomerated powder gives inhomogeneous particle packing structure within the green body and poor green density (green body density to theoretical density). Therefore, to get fully dense structure has some difficulties to achieve. Actually, the success of good green body density depends on the agglomeration level in the starting powder.

Another problem of the compaction of the nanocrystalline powder is the friction forces between each particle during compaction process. Nanocrystalline powder has greater particle-particle contact point when it is compared with the powder having larger particle size. This friction between particles causes application of higher pressures but at the same time applied high-pressure causes the ceramic fracture during subsequent handling or sintering.

Chapter VI

SINTERING BEHAVIOR AND MICROSTRUCTURE OF
NANOCRYSTALLINE CERAMICS

Sintering can be described as reduction of surface energy with the increase temperature. The temperature must be below material's melting point mostly half of the melting point. The mechanism of the sintering process can be described as: Mass transport (mostly, diffusion) that is driven by excess free surface energy associated with surface area of the powder. The difference in the surface curvature where the particles touch each other (negative curvature = neck formation) relative to the rest of the surface of the particle (positive curvature), causes mass to fill the contact region between adjacent particles. If mass is transported from the region between particle centers, mass transport will lead the to the shrinkage and densification. That's why sometimes this process would called as densification. Generally, sintering is done presurelesss so called as pressureless sintering. But recently for a solution of some sintering problem pressure assisted sintering is applied.

There are three stages of pressureless sintering: In first stage, neck growth occurs at the contact points between adjacent particles. The ceramic has a sponge-like structure consisting of an excessive network of tubular pores open to the outside surface of the ceramic sample. In the second stage these pores shrink so they become isolated, become closed spherical pores. So that densification occurs. The elimination of these closed pores takes place in the final stage of sintering as shown in Figure 6.1.

The result of this process is maximizing properties like strength, thermal conductivity, translucency, superplasticity, etc. These kinds of properties improve as the porosity eliminated. The mechanism, which is responsible for the matter flow during sintering, is summarized by Ashby [25] as shown in Table 6.1.

Table 6.1. A brief explanation on the mechanizm of the sintering behavior of the ceramics [14].

Mechanism No	Transport Path	Source of Matter	Sink of Matter
1	Surface Diffusion	Surface	Neck
2	Lattice Diffusion	Surface	Neck
3	Vapor transport	Surface	Neck
4	Boundary Diffusion	Grain Boundary	Neck
5	Lattice Diffusion	Grain Boundary	Neck
6	Lattice Diffusion	Dislocations	Neck
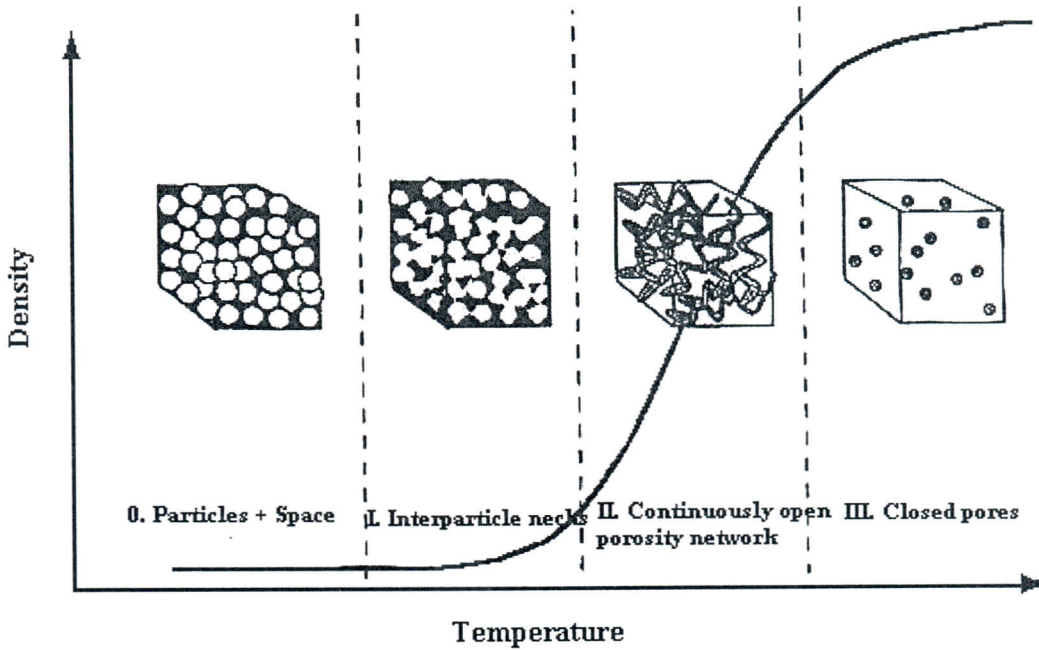
Figure 6.1. Schematic diagram illustrating the three stages of sintering [36].

All mechanisms described on the Table 6.1 is based on the diffusion of the matter into the neck between the powder particles. This may cause the grain growth. In the mechanisms one to three, the source of diffusion is surface only cause the rounding of the pores. In the mechanisms four to six, distance between particles decreases so densification and shrinkage take place.

All these observations of sintering for ceramics explained above are the same for the sintering of nanocrystalline ceramics. However, it is important to keep the grain sizes in nanoscale (below 100 nm) for processing nanocrystalline ceramics. As temperature increases grain growth occurs to minimize the surface free energy. Therefore, sintering temperature must be kept as low as possible with complete sintering to get fully dense nanocrystalline ceramic bodies with an absolute minimum grain growth. As a result, the grain growth must be under control to produce nanocrystalline ceramics. The grain growth occurs in the second stage of sintering so it is the most important stage (see in Figure 6.1.).

It is generally accepted that the densification of a ceramic body or the shrinkage of the pores occurs by diffusion. The driving force of the diffusion is the reduction of the internal surface area associated with the pores [32]. The instantaneous driving force for the diffusion is assumed to be inversely proportional to the pore's radius curvature. A tighter pore curvature sets a higher vacancy concentration in the vicinity of the pore

$$c = c_o \exp\left(\frac{A\gamma}{r}\frac{\Omega}{kT}\right) \approx c_o\left(1 + \frac{A\gamma\Omega}{rkT}\right) \qquad \text{(Eq.6.1)}$$

Here, c_o is the equilibrium vacancy concentration (at temperature) in the bulk material, away from the pore k is Boltzmann's constant, Ω is the atomic volume, r is the pore radius (inverse of pore curvature), γ is the surface tension associated with the pore/solid interface, and A is a geometric constant with a value of 1 (cylindrical pore). The driving force for sintering, or the 'sintering stress', is often written as σ, where

$$\sigma = A\gamma/r \qquad \text{(Eq.6.2)}$$

Using this equation, one can estimate the densification rate of the ceramic body depending on its pore size.

The Herring scaling law is often used to estimate the reduction in pore size or particle size. The driving force is assumed to be the form of Equation 2, which is given as follows

$$\frac{d\rho}{dt} \propto \frac{1}{G^N} \exp\left(-\frac{Q}{RT}\right) \qquad \text{(Eq.6.3)}$$

A rearrangement of the Equation 6.3 then leads to a useful expression of the Herring scaling law

$$\frac{RN}{Q} \ln\left(\frac{G_2}{G_1}\right) = \frac{1}{T_1} - \frac{1}{T_2} \qquad \text{(Eq.6.4)}$$

where G is the particle size of powder 1 or 2, Q is the activation energy for diffusion, R is the gas constant, T is sintering temperature of powder 1 or 2 in degrees Kelvin, and N is a constant which depends on the diffusional path (N=3 for lattice diffusion and N=4 for grain boundary diffusion). But the Herring scaling law is rule of thumb, and the predictions done for full reduction in sintering temperature are rarely achieved. Because, there is no distinction made between grain size and agglomerated/aggregate size.

Therefore, the ability to predict the densification behavior of nanocrystalline ceramics during pressureless sintering is currently poor. The reason is the lack of data on well-characterized nanocrystalline samples sintered under a suitable variety of controlled sintering conditions. However, even for commercial ceramics, there is not an accurate densification relation which predicts the density as a function of time, temperature, and the starting microstructural parameters. Another difficulty is that all these parameter are changed from one powder to another.

$$\frac{1}{\rho(1-\rho)} \frac{\rho}{dt} \propto \frac{1}{G^N} \frac{1}{r} \exp\left(-\frac{Q}{RT}\right) \qquad \text{(Eq.6.5)}$$
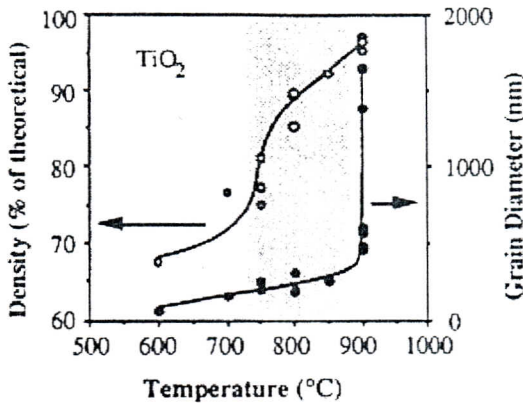
Figure 6.2. Evolution of density and grain growth during the sintering of a nanocrystalline Titania powder [30]

6.1. Characterization and Sintering Behavior of Nanocrystalline Titania and Zirconia

Since the grain growth and densification are driven by the same mechanizm-diffusion- it assume to be reasonable that the two processes would have the same kinetics. For fine-grained powders, both grain boundary area and pore surface area increase with the inverse of grain/particle size. Therefore, it is expected that both grain growth and densification would occur simultaneously and rapidly in nanocrystalline powder compacts. However, for Titania and Zirconia nanocrystalline ceramics, there is a regime that the grain growth remains slow or stagnant while densification proceeds quite rapidly as shown in Figure 6.2. In fact, Titania and Zirconia ceramics have a minimal grain growth in a range of 600-1000°C as shown in Figure 6.3.

It is important to reduce the size and number of pores, to have a successful sintering. Since nanocrystalline powder is very fine, good compaction and low size and number of pores are expected. However, many nanocrystalline powders tend to agglomerate. Individual crystallites are bonded together by chemical or physical forces into larger units in agglomerated powders (see Figure 6.4.).

When the powder is pressed into a compact, the packing of these large agglomerates then leaves behind large interagglomerate pores. The larger the agglomerates, the larger the interagglomerate pores, and the higher the sintering temperatures are needed. The Figure 6.5 is an example of this fact.

As a result, to achieve full-dense or nearly full dense nanocrystalline ceramics, the sintering temperature, pore size distribution, and reduction of agglomerates must be considered.
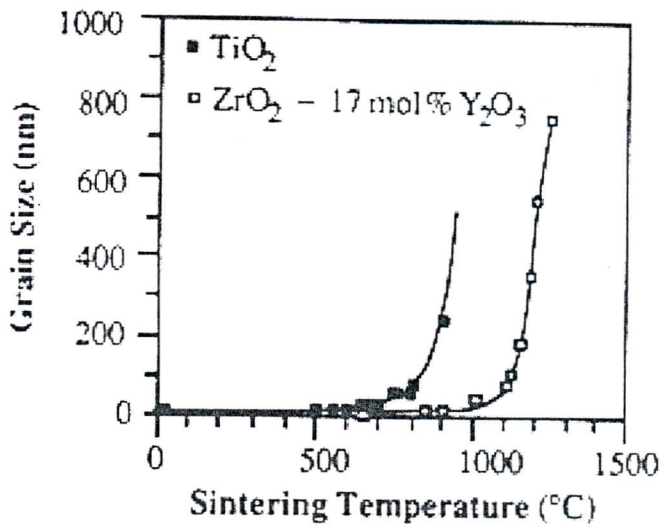
Figure 6.3. Grain growth curves for nanocrystalline titinia and yittria–stabilized Zirconia as a function of sintering temperature [30].
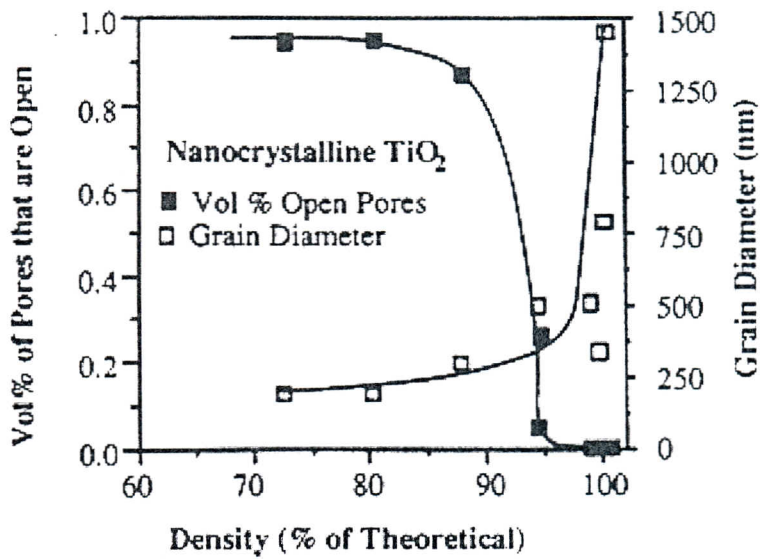
Figure 6.4. Corelation between the closure of open pores and the onset of accelarated grain growth [30].
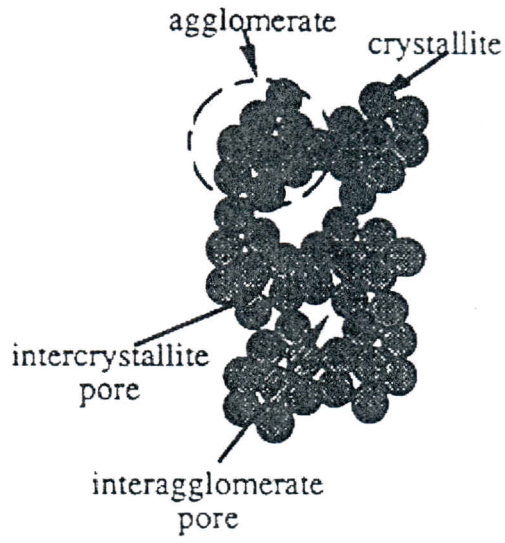
Figure 6.5. Schematic illustration of an agglomerated powder [34].

Chapter VII

EXPERIMENTAL

7.1. Chemicals and Materials

Titania sols were prepared by mixing titanium isopropoxide, 2-propanol and nitric acid solution in predetermined ratios. The physical properties of the materials used in this study is tabulated on the Table 7.1.

Table 7.1. The physical properties of the materials used.

Titanium (IV) Isopropoxide $Ti[OC(CH_3)_2]_4$	97% FG= 284.26 FP=18-20°C Kp=232° Aldrich
2-Propanol $CH_3CH(OH)CH_3$	99.5% M=60.10 1 lt=0.78 kg Merck
Nitric Acid HNO_3	65% m=63.01 g/mol 1 lt=1.40 kg Merck

The physical properties of the additives using for controlling the drying process of the gels is tabulated on Table 7.2.

Table 7.2. The physical properties of the additives.

Stearic Acid (octadecanoic acid) $C_{18}H_{36}O_2$	90% FW=284.4 Sigma
Oxalic Acid $C_2H_2O_4.2H_2O$	99.6% FW=126.1 Aldirch
Polyacrylic Acid	MW=2000 Aldrich
Acetic Acid $C_2H_4O_2$	99% 1lt=1.05 kg MW=60.05 Merck

7.2. Preparation of Sols

The nanocrystalline Titania sols were prepared by hydrolysis of Titanium(IV) Isopropoxide. The following reactions took place during the synthesis:

$$Ti[OC(CH_3)_2]_4 + H_2O \rightarrow TiO_2 + 4(C_3H_7)OH$$

$$Ti[OC(CH_3)_2]_4 + 4 H_2O \rightarrow Ti(OH)_4 + 4(C_3H_7)OH \quad hydrolysis$$

$$Ti(OH)_4 \rightarrow TiO_2 + 2H_2O \; condensation$$
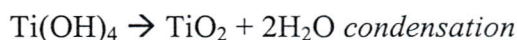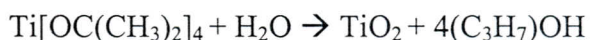
Predetermined amounts of titanium (IV) isopropoxide were diluted with half of the required amount of 2-propanol. 1.44 M prepared nitric acid solution was mixed with the remaining amount of the total 2-propanol so the required amount of water for the hydrolysis reaction was supplied from the acidic solution. The acid-alcohol solution was added to the alkoxide-alcohol solution slowly while the mixture was stirred vigorously with a magnetic stirrer.

Initially, 10 sol samples were prepared by changing the amount of Titanium (IV) Isopropoxide. The determined amounts of the materials used for sol preparation are tabulated in Table 7.3. It was observed that the sols having TiO2 content higher than the TC8 sol was precipitated and no longer clear. The TC8 sol was blurry and gelled in approximately two hours. Therefore, TC6 was chosen by compromising clarity, gelation time and TiO_2 content of the sols.

Table 7.3. The determined ratios and values of the Titanium (IV) Isopropxide, Isopropanol and 1.44 M Nitric Acid Solution that were used during the preparation of the Titania sols.

TC Series	Ti(IV) IP (ml)	The Constant Ratios			n_{Ti} (mol)	n_{H2O} (mol)	V_{HNO3} (ml)	V_{2-P} (ml)	M_T (g)	Ti%wt
		H_2O/Ti	H^+/Ti	2-P/Ti						
TC1	2.5	2	0.0537	100	8.15 E-3	4.38 E-4	0.303	62.8	65.50	0.994
TC2	5	2	0.0537	50	0.0162	0.0326	0.607	62.8	54.38	2.39
TC3	7.5	2	0.0537	40	0.0224	0.0488	0.908	75.2	66.76	2.92
TC4	10	2	0.0537	30	0.0326	0.0652	1.21	75.4	69.59	3.74
TC5	12.5	2	0.0537	25	0.0407	0.0814	1.52	78.4	73.66	4.41
TC6	15	2	0.0537	20	0.0489	0.0978	1.82	75.4	74.99	5.21
TC7	17.5	2	0.0537	15	0.057	0.114	2.12	65.9	70.30	6.49
TC8	20	2	0.0537	10	0.0652	0.1304	2.43	50.2	60.79	8.57
TC9	22.5	2	0.0537	8	0.0733	0.1466	2.73	45.2	59.37	9.87
TC10	25	2	0.0537	5	0.0815	0.163	3.03	31.4	51.51	12.64

7.3. Drying of the Gels

Gelation process of the sols was performed by aging at room temperature. After the gelation of the sols in 5-6 days, drying process was carried out. The gels were dried by both keeping at room temperature or in vacuum oven at 40°C to form a monolith. The drying process of the gels was very slow. The gels tend to crack easily so the rate of the solvent evaporation must be slow. The shrinkage of the gel occurred in large scale during the drying process. Thus, the shape of the gels did not remain steady.

In order to control the drying of the gels and to avoid extend cracks, some drying control chemical additives (DCCAs) were introduced to the sols about one or two weight percents. The solutions of the DCCAs were prepared in alcohol, which are listed in Table 7.2. After preparation of the sol, the DCCA solutions were added slowly while the mixture was stirred with a magnetic stirrer.

7.4. Powder Preparation

Agglomeration is one of the major problems of nanocrystalline ceramic powder processing. It influences not only the success of the compaction of powder but also sintering of the powder compacts. Different powder preparation routes were investigated in this study in order to minimize the agglomeration problem.

Generally gels were dried and then ground in a mortar manually then different techniques were applied to achieve as smaller powder particle size as it could be. The basic steps of the powder preparation methods are given schematically in Figure 7.2.

In Route 1, powder was prepared by precipitation of TC6 sol in large quantity of water. In this route, firstly the sol was kept at room temperature for a day in order to stabilize the chemical and physical properties before the precipitation operation. While the mixture was stirred by a magnetic stirrer, the sol was dropped into large quantity of water. Precipitation was occurred simultaneously and the precipitate was separated by centrifuge. The cake was dried at 70°C, subsequently ground in a mortar manually. The calcination of the powder was carried out at 400°C for two hours.

Drying of the TC6 gel at 80°C for ten hours is the first step of the Route 2. The dried gel pieces were ground in a mortar manually and the ball mill was applied for seven

hours in alcohol medium to reduce the powder particle size. Then the suspension was dried at 70 °C and pre-calcinated at 200 °C for two hours. The ball-milling step was applied under the same conditions of the previous ball milling operation. The suspension was dried at 70°C. Finally the powder was calcinated at 400°C.

Route 3 was similar to Route 2. After preparation of the sol and gelation of the sol, the gel was dried at 80°C for ten hours and ground in ball mill for 12 hours in an alcohol medium. The mixture was dried at a temperature of 110°C for 15 hours. The calcination step of the powder was carried out at 400°C for two hours.

Route 4 was based on powder preparation from TC6 gels. Following gel drying at 175°C for about ten hours, and the pieces were ground in a mortar. Then ball milling of medium size gel pieces was conducted in an alcohol medium for 12 hours. The mixture of gel powder and alcohol was kept in an ultrasonic bath for five hours and subsequently dried at a temperature of 70°C. Finally, the prepared powder was calcinated at 400°C for two hours.

The produced powders by these four different preparation techniques were dry pressed to form pellets in about 1 mm thickness and about 10 mm diameter. The pressure applied on the pellets was 318 MPa. Also the pressure effect on the relative density was studied. The applied pressures were varied between 304-608 MPa.

Gels and pellets were sintered in a chamber furnace (Carbolite 1600 RHF 16/3c) at 650, 700, 750, 800 and 850°C. The heating and cooling rates(10°C/minute) and soaking time (2 hours) were kept constant for the all sintering processes.

7.5. Characterization

The density measurements of the sintered gels and pellets were carried out in Sartorius YD01 density measurement kit (see Appendix 1). The TGA curves were achieved by Thermalgravimetric Analyzer (TGA-51/51H, Shimadzu Co.). The carrier gas is nitrogen with a flow rate of 15 ml/min. and the heating rate is 10 °C/min. The pore size distribution information was observed by Micromeritics-ASAP 2010. The absorptive is N_2. The FTIR Spectrum was achieved by Fourier Transform Infrared Spectroscopy (FTIR-1600, Shimadzu Co.). The samples were prepared by pressing samples which were ground with dried crystalline KBr. The samples were approximately 4 mg in 200 mg KBr. The

micro-hardness strength of the sintered pellets and the dried gels were measured by Vickers Micro-Hardness Tester (HVS-1000). SEM pictures were taken by Jeol 5200 provided by the Dentistry Faculty of Ege Univetsity.
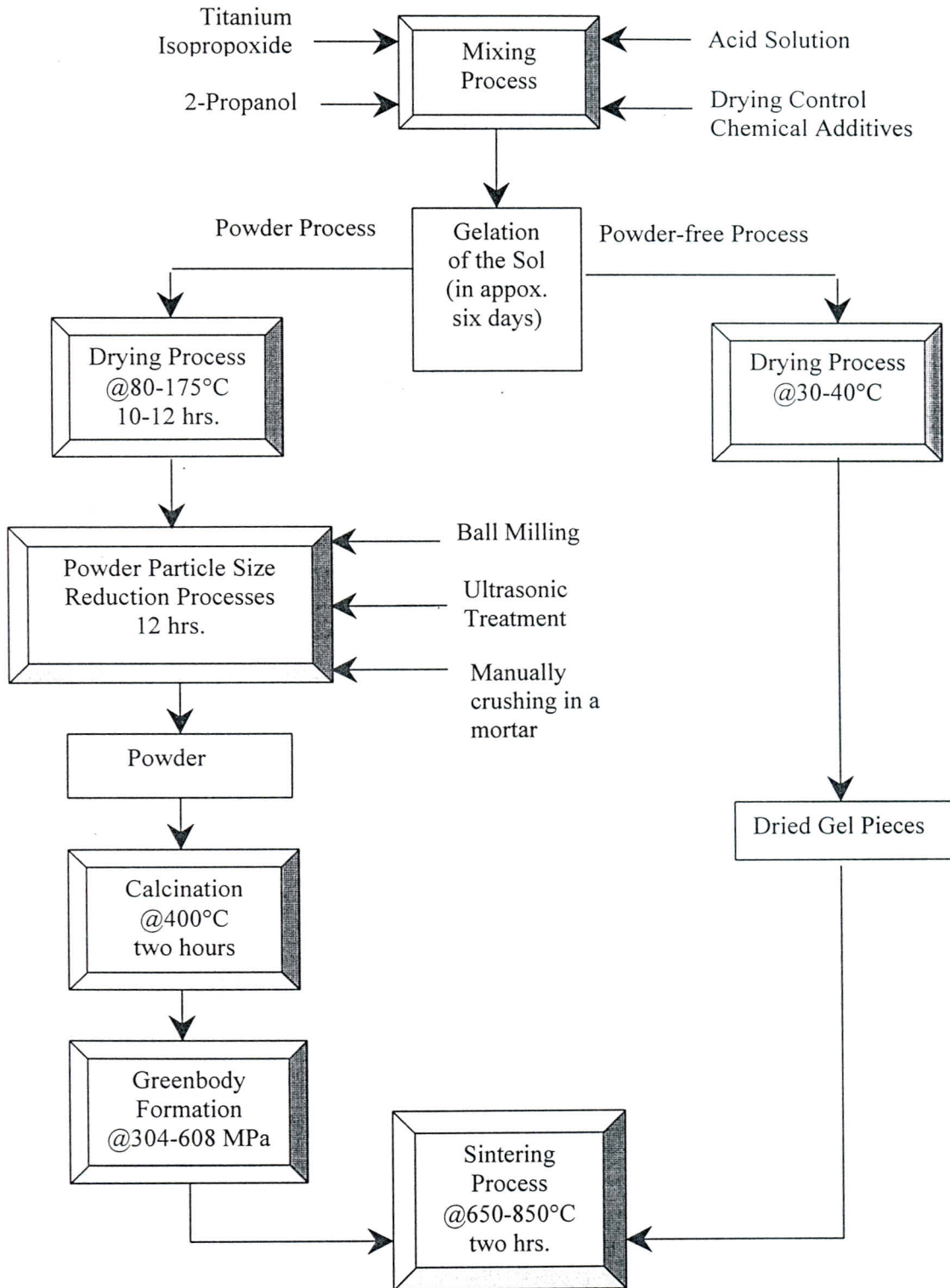
Figue 7.1. Flowsheet of the sol-gel process and experimental procedure.

ROUTE 1:

Mixing → Precipitaion → Seperation by centrifuge → Drying @70°C

↑ TC6 sol ↑ Bidistillated Water (into Mixing)

Drying @70°C → Grinding in mortar manually → Calcination @400°C → Final Powder

ROUTE 2:

TC6 Gel → Drying @80°C → Grinding in mortar → Ball Milling Seven hrs.

Ball Milling Seven hrs. → Drying @70°C → Pre-calcination @200°C two hrs. → Ball Milling Seven hrs. → Drying @70°C

Drying @70°C → Calcination @400°C two hrs. → Final Powder

ROUTE 3:

TC6 Gel → Drying @80°C → Ball Milling 12 hrs. → Drying @70°C → Calcination @400°C → Final Powder

ROUTE 4:

TC6 Gel → Drying@175°C 10 hrs. → Grinding in a mortar manually → Ball Milling 12 hrs. → Ultrasonic Treatmant 5 hrs

Ultrasonic Treatmant 5 hrs → Drying@70°C → Calcination @400°C → Final Powder
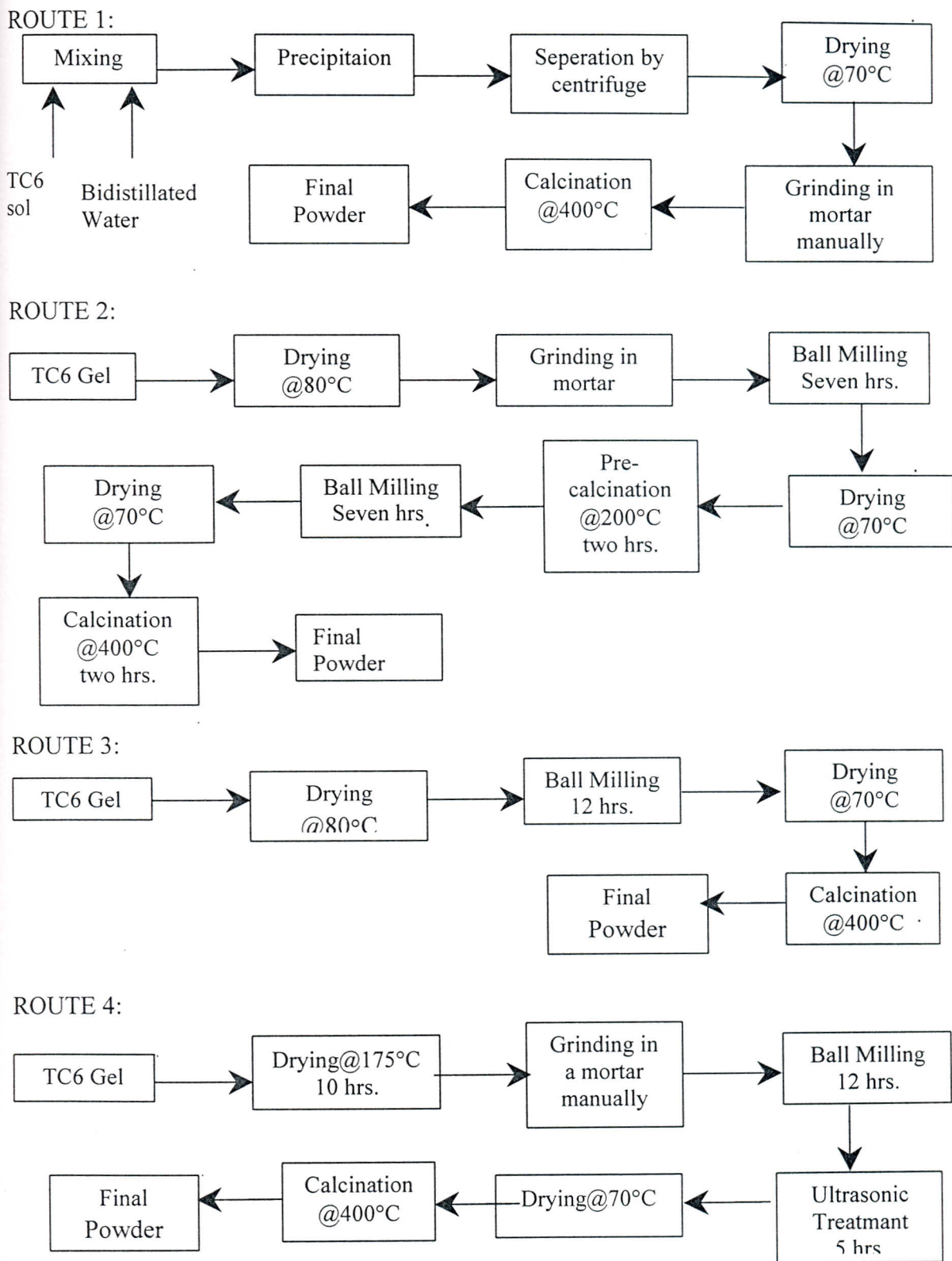
Figure 7.2. Flowsheets of the powder preparation techniques used in this work.

Chapter VIII

RESULTS AND DISCUSSION

Titania sols were prepared by using Titanium (IV) Isopropoxide, Isopropanol and Nitric Acid solution. During the preparation of Titania sols, Titanium (IV) Isopropoxide was diluted with half of the required amount of Isopropanol. 1.44 M nitric acid solution was prepared. The pre-determined amount of the acid solution was mixed with the remaining amount of the total Isopropanol so that the required amount of water for the reactions was supplied from the acidic solution. The acid-alcohol mixture was added to the alkoxide-alcohol mixture slowly while the mixture was stirred vigorously with a magnetic stirrer. The direct introduction of the acidic solution to Titanium (IV) Isopropoxide-Isopropanol mixture resulted in precipitation. It was observed that the sols having TiO_2 content higher than the TC8 sol (see Appendix 1) contained precipitates and was no longer clear. The TC8 sol was blurry and gelled in approximately one or two hours. Therefore, TC5 and TC6 sols were chosen for the preparation and characterization of nanocrystalline Titania comparing the clarity, gelation time and TiO_2 content with the other sols.

Two different techniques were used for the preparation of fully dense nanocrystalline Titania. The first technique contained the drying process of gels as a monolith and subsequent sintering. The second technique was the powders preparation from sols and dried gels. The powders prepared by different techniques were compacted and subsequently sintered. These techniques were described in detail in Figure 8.1 and Figure 8.2.

8.1. Powder-free Technique

In the first technique, the drying process of the gels was very slow. The gels tend to crack easily so the rate of the solvent evaporation must be kept very low. The drying process was lasted three to four months. The shrinkage of the gel occurred in large scale during the drying process because of the low TiO_2 content in high volume of Isopropanol. Thus, the shape of the gels didn't remain steady and they were divided into several pieces because of the rate of the solvent removal. In order to prevent the excess cracks, some chemicals that are known as drying control chemical additives (DCCAs) were added during the preparation of sols. Generally, as the amount of the DCCA was increased, the gelation time of the sol was

decreased. One of the used DCCAs was polyacrylic acid. The addition of one weight percent polyacrylic acid accelerated the gelation process. The sol was gelled in one or two days. The addition of two weight percent polyacrylic acid made the sol blurry and gelled in two hours. The second DCCA was oxalic acid. The addition of one weight percent oxalic acid didn't influence the gelation time of the sol but two weight percent of the oxalic acid solution completed the gelation in two days and made the sol blurry. The third used DCCA was acetic acid. One and two weight percent of the acetic acid solution didn't influence the gelation time and the clarity of the sol. On the contrary, the stearic acid addition as DCCA stopped the gelation process. The sols with one and two percent of stearic acid didn't gelled in 40 days after the addition. After the addition of three and four percent of the stearic acid solution the sol became nearly white opaque, but during the addition of the stearic acid the clarity of the sol didn't change. However, the appearance of the sol turned into white opaque in time after the addition. The reason of the gelation hindering and the change in the appearance and clarity of the sol might be blocking the molecular interactions between the particles because of the big molecular size of the stearic acid. Stearic acid solution precipitated at room temperature. The solubility of the acid increases as temperature increases. Therefore, the stearic acid precipitated when the temperature decreased and virtuously stirring was stopped.

The dried gel pieces with and without DCCAs were sintered at different temperatures and then the densities were measured. The measured densities of the sintered gel pieces is given in the Table 8.1.

Table 8.1. Density Measurements of the Sintered Gel (TC6) Pieces without any DCCA.

Density Measurements of the Sintered Gel (TC6) Pieces without any DCCA					
Sample Number	Sintered Temperature(°C)	Wd (g)	G (g)	$**\rho$ (g/cm^3)	Relative Density wt-%
1	650	0.1769	0.0464	3.79	79
2	700	0.2215	0.0561	3.86	91
3	700	0.1685	0.0427	3.91	92
4	750	0.4172	0.1027	4.02	94
5	750	0.1901	0.047	3.99	94
6	800	0.9723	0.0908	4.12	97
7	800	0.1753	0.0421	4.02	94
8	850	0.2496	0.0598	4.16	98.4
9	850	0.3534	0.0841	4.19	99

Table 8.2. Density measurements of the Sintered Gel Pieces with DCCAs

| Density Measurements of the Sintered Gel Pieces with DCCAs					
TC6 with 1 wt-% Oxalic Acid					
Sample Number	Sintered Temperature(°C)	Wd (g)	G (g)	$**\rho$ (g/cm^3)	Relative Density wt-%
1	650	0,41	0,10	3,96	93,06
2	700	0,68	0,17	4,08	95,75
3	750	0,64	0,15	4,15	97,52
4	800	0,74	0,18	4,19	98,30
5	850	0,37	0,09	4,19	98,45
TC6 with 2 wt-% Oxalic Acid					
Sample Number	Sintered Temperature(°C)	Wd (g)	G (g)	$**\rho$ (g/cm^3)	Relative Density wt-%
1	650	0,17	0,04	3,93	92,28
2	700	0,34	0,09	3,94	92,50
3	750	0,35	0,09	4,08	95,89
4	800	0,29	0,07	4,19	98,44
5	850	0,47	0,11	4,20	98,60
TC6 with 1 wt-% Polyacrylic Acid					
Sample Number	Sintered Temperature(°C)	Wd (g)	G (g)	$**\rho$ (g/cm^3)	Relative Density wt-%
1	650	0,20	0,05	3,97	93,29
2	700	0,08	0,02	4,14	97,19
3	750	0,12	0,03	4,14	97,27
4	800	0,17	0,04	4,18	98,03
5	850	0,08	0,02	4,18	98,10
TC6 1 wt-% Acetic Acid					
Sample Number	Sintered Temperature(°C)	Wd (g)	G (g)	$**\rho$ (g/cm^3)	Relative Density wt-%
1	650	0,12	0,03	4,12	96,65
2	700	0,06	0,01	4,12	96,79
3	750	0,11	0,03	4,16	97,70
4	800	0,13	0,03	3,99	93,63
5	850	0,15	0,04	4,09	96,06
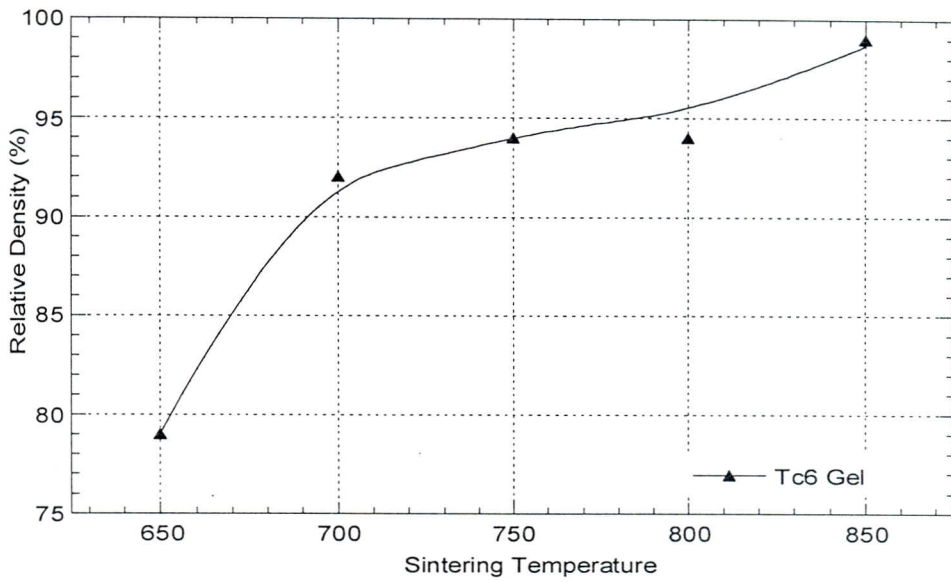
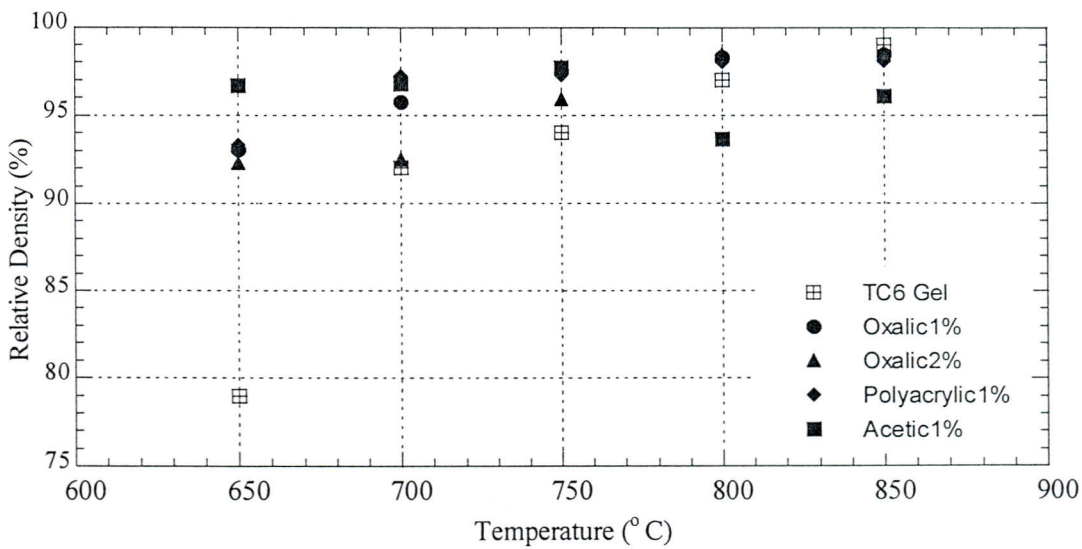Figure 8.1. The densification behavior of TC6 gel without any DCCAs.

Figure 8.2. Densification Behaviors of TC6 gel and TC6 gels with different DCCAs.

48

Figure 8.1 shows the densification results of TC6 Titania gel pieces. The relative densities of the sintered Titania increased with the sintering temperature. The densification rate accelerated between 650°C and 700°C but decreased after the temperature of 750°C.

The dried gel pieces with DCCAs showed approximately same densification behavior with the gel pieces without DCCAs as shown in Table 8.2 and Figure 8.2. Actually the densification behaviors of the sintered gel pieces with DCCAs seem to be inconsistent. This inconsistent behavior might be the result of following several reasons. The gels were divided into several small pieces during drying that have small weights as it is shown on the Table 8.2. There were some macro-cracks that could be detected by eye on the pieces and also there might be some micro-cracks. These possible micro-cracks would be the result of the decomposition of organics present in the gel during sintering process.

TGA curves show the weight loss of the gel pieces versus temperature in Figure 8.3. The gel with acetic acid had the highest weight loss with respect to the others. The decomposition of organics was completed 400-425°C for TC6 gel and TC6 gels with oxalic acid one wt-% and polyacrylic acid one wt-% but this step was continued up to 450°C for TC6 gel with acetic acid one wt-%. The decomposition of organics in the gel with acetic acid one wt-% was the fastest with respect to the others. This relatively fast decomposition of organics caused the sintered gels to break into small pieces or caused micro-cracks. This fact might be the reason of the low densities and/or inaccurate density measurements or inconsistence densification behaviour of Titania gel with acetic acid.

The gels with polyacrylic acid reached lower densities than the others as it is shown in Figure 8.2. Polyacrylic acid has bigger molecule than the other DCCAs thus higher amount of gas releases during the decomposition. This fact may cause the formation of the pores in the sintered pieces.

The gels with oxalic acid had a better densification behaviour with respect to the other samples. TC6 Titania samples with one wt-percent and two wt-percent oxalic acid had the approximately same densification behaviour. The density values were about the same.
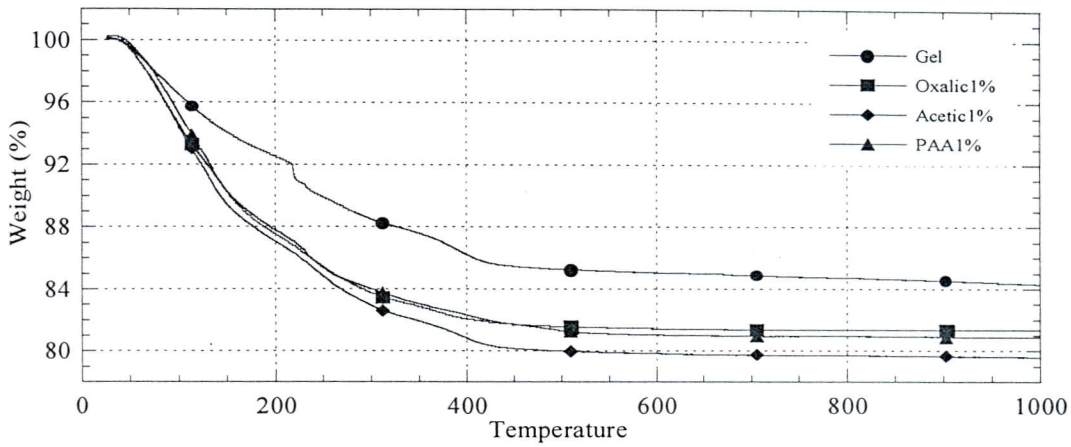
Figure 8.3. TGA Curves of TC6 Gel and TC6 Gels with Oxalic Acid, Acetic Acid and
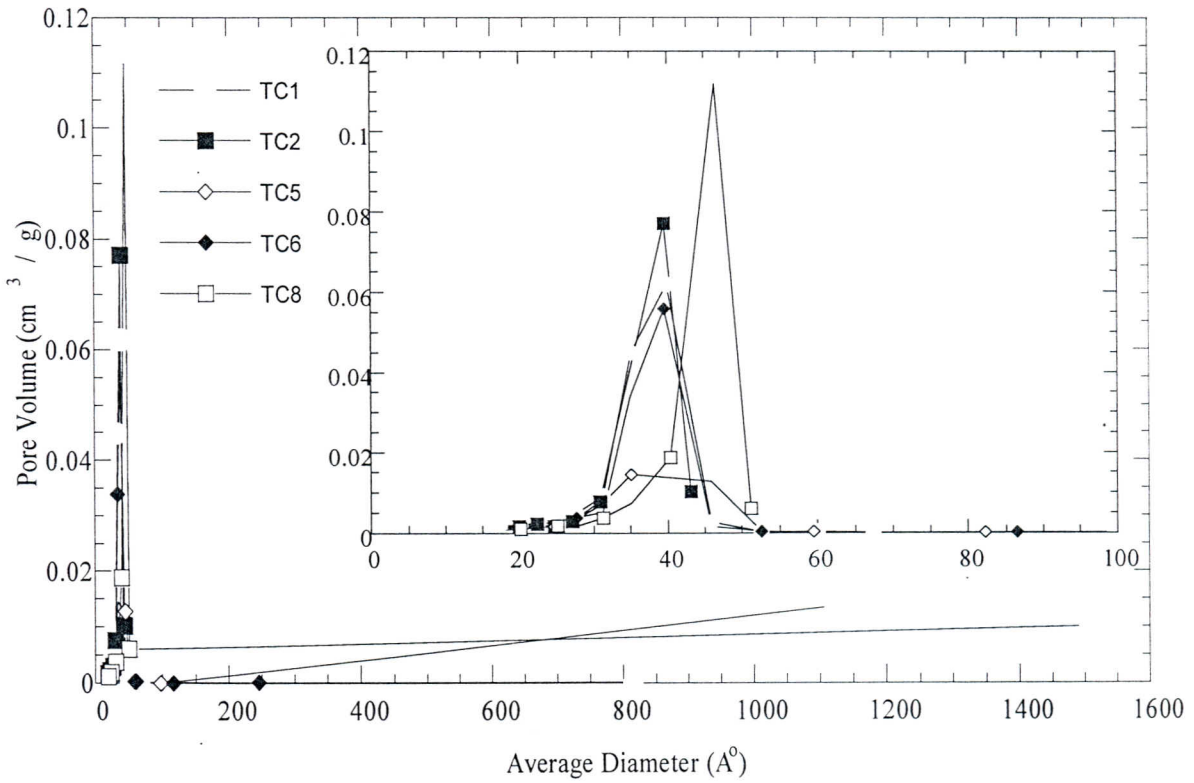Polyacrylic Acid

Figure 8.4. The pore size distribution of TC1, TC2, TC5, TC6, and TC8 gels.

The pore size analysis of the Titania dried gels is shown below in Figure 8.4. These sharp peaks located at small radii indicate that there were only small pores, which didn't vary. The single peak at small radii meant that there weren't any agglomeration in gels as expected. If there were secondary peaks which were located at larger radii, there would be interagglomerates. According to the data of pore size analysis, the relative density of dried gels could be determined by a simple calculation. The analysis gave the total amount of the pores at different diameters in cm^3 per gram. The relative density can be calculated by subscribing the pore volume from the theoretical volume. According to this simple calculation, the relative density of the gel was calculated as approximately 70%.

8.2. Powder-based Techniques

Several different processing paths were followed in this work. The aim of developing these techniques was to prepare non-agglomerated nano-sized powders which were used for the preparation nanocrystalline ceramics. In these techniques, the Titania sols and gels were used. The powder preparation techniques were described in detail in the experimental work section.

The calcination temperature was determined from the TGA curves. Figure 8.5. shows that the weight loss became stable around 400°C hence the calcination was performed at 400°C for two hours.

The effect of compaction pressure on sintered density is given in Table 8.3 and shown graphically in Figure 8.6. The sintering temperature of the powder compacts was 700°C. The compaction pressure increased from 304 to 608 MPa, the green-body density increased from 43 to 48% and the relative density increased from 65 to 78%. The pressure increment was also effected to open and closed pores of the powder compacts. The open pore percent of the compacts reduced from 39 to 13 and with a basic calculation closed pore percent reduced from 10.9 to 0.9.
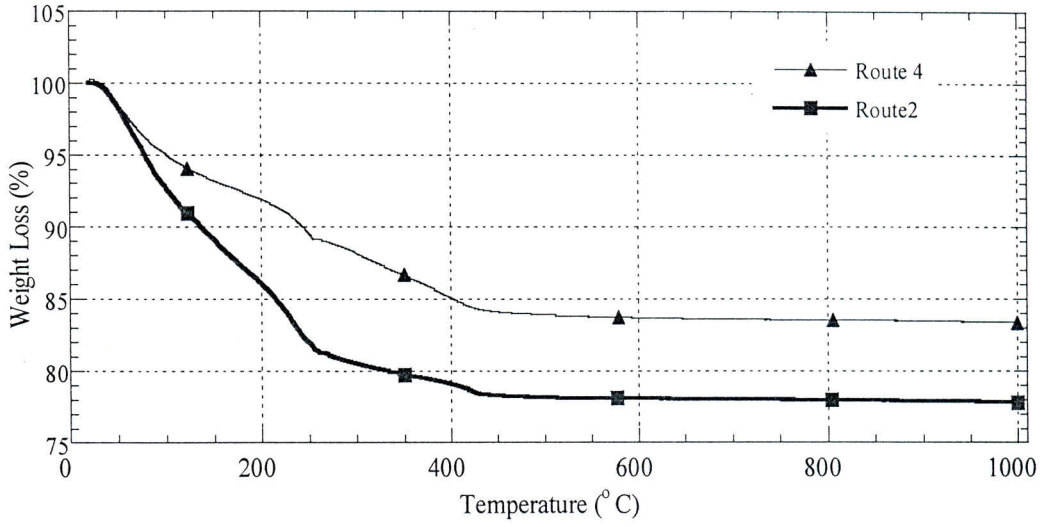
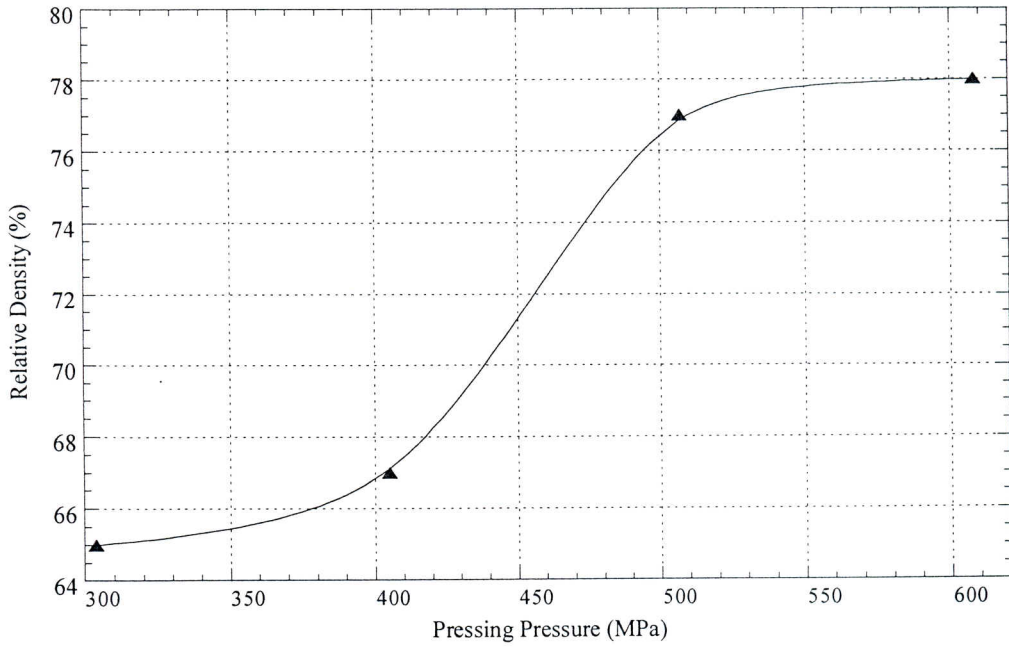Figure 8.5. TGA curves of Route3 and Route5.

Figure 8.6. The Relative Density versus Pressure Graph of Route 4

(The Sintering Temperature of the Compacts was 700 °C).

Table 8.3. Density Measurements of the Pellets before and after sintering at 700°C.

| Pressing Pressure Mpa | Before Sintering | | | | | After Sintering | | | | | Open Pore % |
	W (g)	D (cm)	H (cm)	ρ^* (g/cm^3)	RD %	W (g)	W_s (g)	W_{ss} (g)	ρ^{**} (g/cm^3)	RD %	
304	1.01	1.41	035	1.86	43	0.969	1.06	0.71	2.75	65	26.26
21.12	1.01	1.41	0.33	1.95	46	0.96	1.05	0.71	2.87	67	27.03
17.12	0.99	1.41	3.07	2.06	49	0.94	1.0	0.72	3.3	77	21.12
7.63	0.89	1.41	0.28	2.03	48	0.74	0.78	0.55	3.15	74	17.21
608	0.467	1.42	0.14	2.04	48	0.44	0.45	0.32	3.34	78	7.63

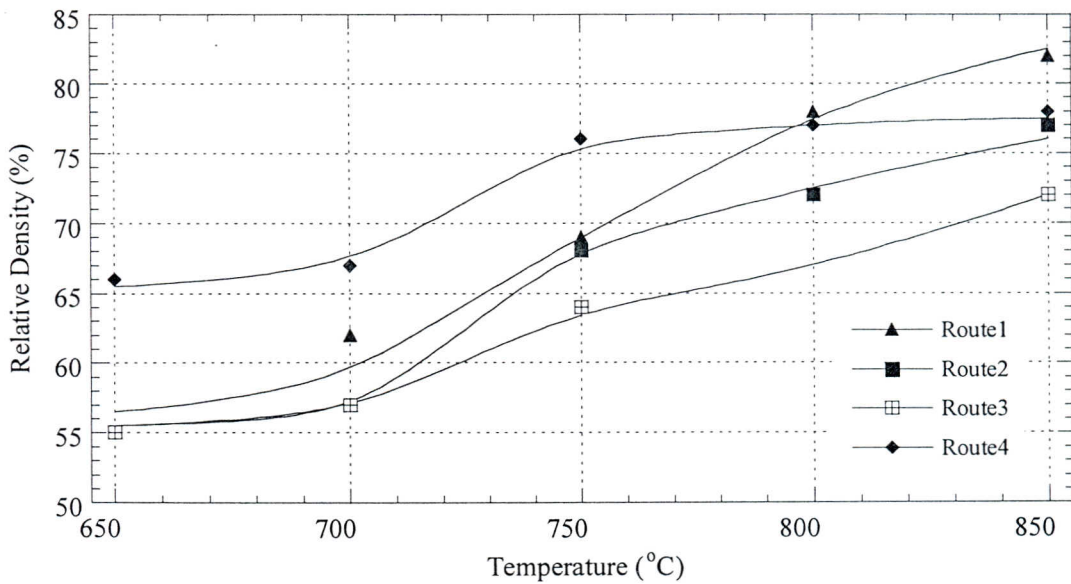(The pellets were produced by Route 4 and they were pressed at different pressures by hydrolic press).

Figure 8.7. The densification behaviour of the pellets produced from Route 2, Route3, Route4, and Route 5.

Table 8.4 (continued)

The Powder Prepared by Route 3												
R4-1	650	0,4545	1,011	0,26	2.09	49	0,4416	0,4956	0,3230	2.34	55	28.9
R4-2	650	0,4567	1,01	0,266	2.13	50	0,4502	0,5107	0,3305	2.37	56	32.4
R4-3	700	0,4575	1,014	0,27	2.15	51	0,4423	0,4993	0,3257	2.41	57	31.6
R4-4	700	0,4641	1,01	0,255	2.05	48	0,4601	0,5172	0,3396	2.40	57	30.4
R4-5	750	0,4804	1,009	0,27	2,22	52	0,4239	0,4739	0,3174	2,69	63	32
R4-6	750	0,4635	1,01	0,258	2,24	53	0,4496	0,498	0,3343	2,73	64	29.6
R4-7	800	0,4765	1,011	0,273	2,17	51	0,4804	0,5142	0,3486	2,89	67	20.3
R4-8	850	0,4748	1,01	0,278	2,13	50	0,459	0,5073	0,3448	2,81	66	29.9
R3-9	850	0,4565	1,014	0,271	2,08	49	0,4371	0,4813	0,3393	3,06	72	31.3
The Powder Prepared by Route 4												
R5-1	650	0,4954	1,009	0,321	1.93	45	0,4374	0,477	0,321	2.79	66	25.7
R5-2	650	0,4626	1,01	0,316	1.83	43	0,4614	0,504	0,3389	2.78	65	25.8
R5-3	700	0,4979	1,01	0,317	1.96	46	0,4738	0,5155	0,35	2.85	67	25.4
R5-4	700	0,497	1,01	0,315	1.97	46	0,4725	0,5116	0,3493	2.90	68	24.2
R5-5	750	0,499	1,01	0,317	1.97	46	0,4682	0,4978	0,3529	3.22	76	20.7
R5-6	750	0,4809	1,01	0,316	1.90	45	0,4558	0,4863	0,3446	3.20	75	21.6
R5-7	800	0,4948	1,01	0,312	1.95	46	0,4692	0,501	0,3584	3.28	77	22.5
R5-8	850	0,4779	1,01	0,301	1.91	43	0,4208	0,4489	0,3205	3.26	77	22.1
R5-9	850	0,4428	1,01	0,316	1.93	44	0,4576	0,4863	0,3489	3.32	78	21.1

Table 8.4. Density Measurements of the Produced Pellets by Different Techniques Before and After Sintering at Different Temperatures

Sample Name	Sintering Temperature (°C)	Before Sintering					After Sintering					Open Pore %
		Wd (g)	D (cm)	H (cm)	ρ (g/cm³)	RD %	Wd (g)	Ws (g)	Wss (g)	ρ (g/cm³)	RD %	
The Powder Prepared by Route 1												
R2-1	650	0,5065	1,012	0,346	1.82	43	0,4822	0,5582	0,3526	2.34	55	37.3
R2-2	650	0,3818	1,011	0,268	1.78	42	0,3651	0,4228	0,277	2.49	58	39.4
R2-3	700	0,5231	1,018	0,363	1.77	42	0,4954	0,5529	0,3659	2.64	62	30.9
R2-4	700	0,5066	1,013	0,341	1.84	43	0,4813	0,5495	0,3539	2.45	57	34.8
R2-5	750	0,5204	1,011	0,368	1.76	41	0,4913	0,5329	0,3662	2.94	69	25.1
R2-6	800	0,5208	1,007	0,356	1.84	43	0,4888	0,518	0,3696	3.28	77	19.8
R2-7	800	0,5156	1,009	0,347	1.86	44	0,4842	0,512	0,3666	3.32	78	19.3
R2-8	850	0,5588	1,01	0,359	1.94	46	0,4852	0,5102	0,3730	3.53	83	18.4
R2-9	850	0,5521	1,01	0,377	1.83	43	0,4937	0,3775	0,5192	3.47	82	13.1
The Powder Prepared by Route 2												
R3-1	650	0.4460	1.008	0.268	2.08	49	0.4268	0.4882	0.3068	2.34	55	34.1
R3-2	650	0.4649	1.012	0.272	2.12	50	0.4465	0.5094	0.3219	2.37	56	34
R3-3	700	0.4578	1.011	0.265	2.15	50	0.4408	0.5016	0.3197	2.41	57	33.8
R3-4	700	0.4755	1.023	0.283	2.04	48	0.4571	0.5210	0.3317	2.40	57	34.3
R3-5	750	0.4487	1.011	0.267	2.09	49	0.4318	0.4835	0.3357	2.91	68	35
R3-6	750	0.4461	1.014	0.266	2.08	49	0.4291	0.4752	0.3279	2.90	68	31.4
R3-7	800	0.4798	1.012	0.271	2.20	52	0.4572	0.5041	0.3548	3.05	72	31.7
R3-8	800	0.4801	1.009	0.274	0.19	51	0.4618	0.5088	0.3614	3.12	73	31.9
R3-9	850	0.4552	1.011	0.268	2.12	50	0.4398	0.4799	0.3456	3.26	77	30.2
R3-10	850	0.4664	1.009	0.261	2.23	52	0.4425	0.4819	0.3446	3.21	75	28.7

The Table 8.4 shows the results of green-body density, sintering temperature, relative density and open pore percent of powder compacts produced by different techniques. Figure 8.7 shows the sintering behavior of the produced powder compacts. The all powder compacts were pressed at 304 MPa.

The pellets produced pellets by Route 1 were sintered between 650 to 850°C. The green-body density of the pellets were varied between 41-46%. Increase in the sintering temperature improved the relative density, open and closed pore percent. When the sintering temperature of the pellets was increased 650 to 850°C relative density increased 55 to 82%, the open pore percent on the surface of the pellets was decreased 39.4 to 13.1% and the closed pore percent was also varied between 4.9 to 2.6.

The green-body densities of the Route 2 pellets were varied between 49 and 52%. The relative density of the pellets sintered at 650°C was about 56%. As the sintering temperature was increased, the relative densities were improved. At 850°C, the relative density was increased to 77%. The open pore and closed pore percent was decreased 34.1 to 20.7 and 10.9 to 4.3 respectively.

The pellets produced by Route 3 technique had a green-body density varied between 49-53%. The densification of the Route 3 was approximately the same with Route 2. The relative density was 55% at 650°C and 72% at 850°C. The open and closed pore percent of the pellets were 32.4 and 11.6 at 650°C and 29.9 and 4.1 at 850°C.

The Route 4 pellets had green-body densities varied between 43 and 46%. After the sintering process, relative densities were 65% at 650°C and 78 at 850°C. The open and closed pores percent were improved as 25.7 and 8.3 at 650°C and 21.1 and 0.9 at 850°C.

There is a significant difference in sintering behavior between the gel-derived Titania and the powder-based Titania. The sintered gels reached higher densities that near to theoretical density of TiO_2. The reason may be the difference in the relative density. The dried gels having significantly higher relative density than the pellets have. The higher relative density may be caused by the lack of agglomeration and very small pore size in the gels. The high relative density might make the elimination of pore easier so the gels reached to the densities that are very close to the theoretical density. Figure 8.8. shows the surfaces of TC6 gel-derived Titania and powder-derived Titania (Route 1) sintered at 850°C.

The hardness of the sintered gel and pellets produced by Route 1 were determined by Vicker's Microhardness Test. Figure 8.9 shows the significant difference Vicker's hardness strength between the sintered gel and pellets. There is approximately 900 MPa difference in Vicker's hardness strength at all sintering temperatures. The hardness strength increases slightly with the increment in the sintering temperature for both gels and pellets. The optical microscope photographs in Figure 8.10 shows the surface of the samples that were sintered at 850°C.
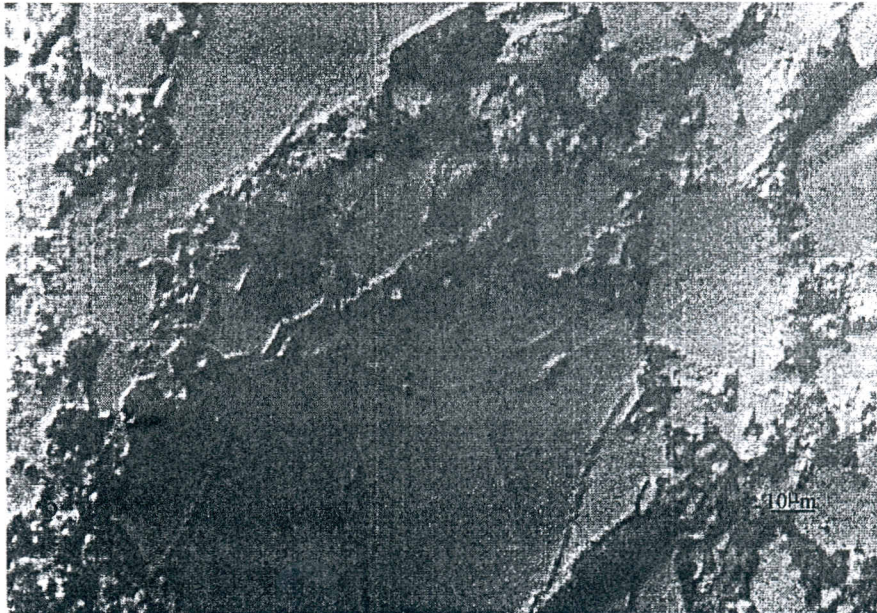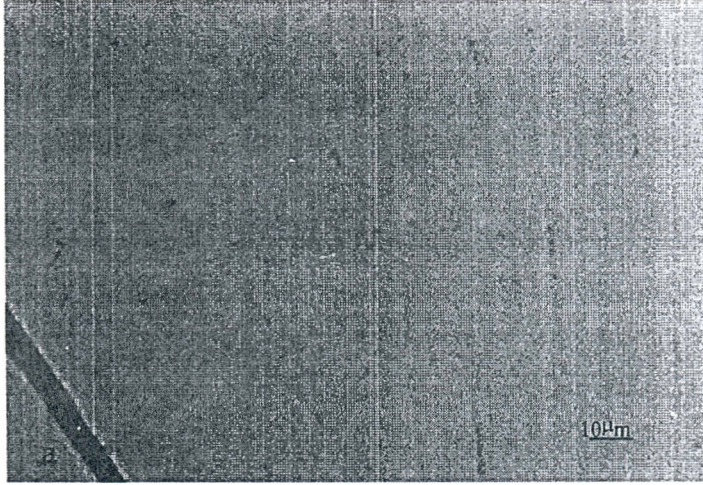
Figure 8.8.The optical microscope photographs at a magnification of 750x.
(a) TC6 gel and (b) pellet of Route 1 sintered at 850°C.
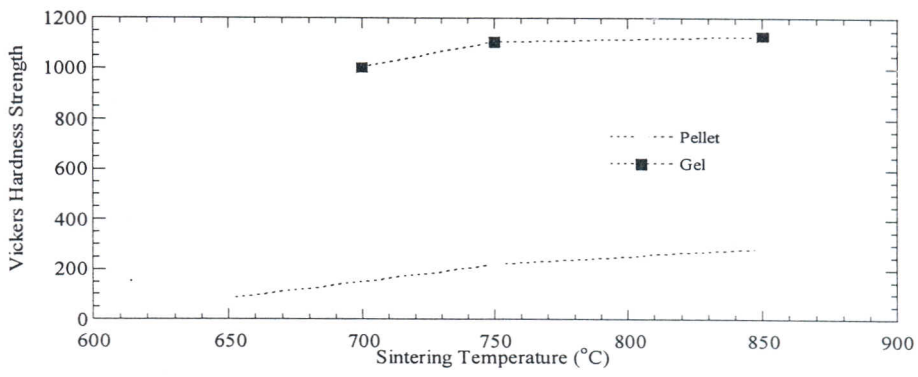
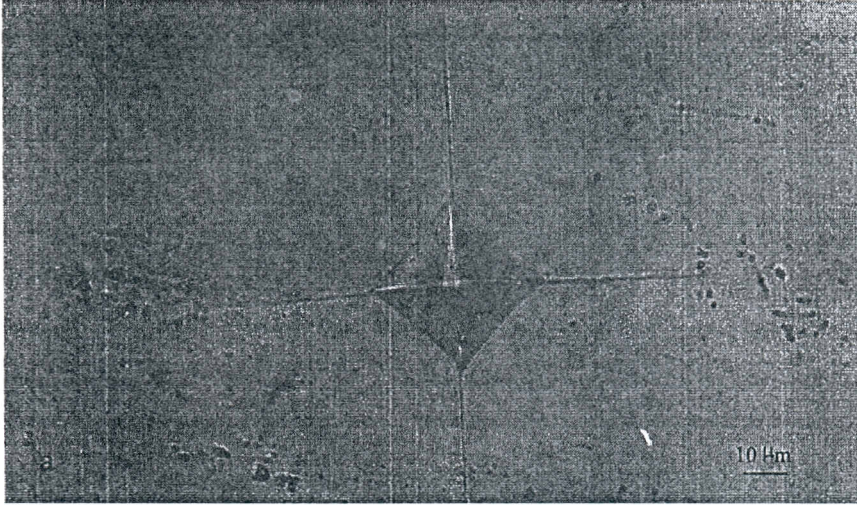Figure 9.9. Vickers Hardness Test results of TC6 gel and Route 1.

Figure 8.10. The optical microscope photographs of (a) TC6 gel and (b) pellet of Route 1 under 750 magnification.

8.4. SEM Analyses

The micrographs of the sintered gel at 700°C were performed by Jeol 5200 which is provided by The Faculty of Dentistry at Ege University. A crack was observed on the surface of the gel that is about 20μm in wide as shown in Figure 8.11. The micrograph was taken at a magnification of 500x (20kV). It is observed that there are some very smooth regions on the irregular surface. Therefore, powder like pieces were not considered as grains. They might be agglomerates attached to the surface somehow. Figure 8.12 shows a micrograph taken at 2000x magnification. A sponge like surface was observed and there are some defects on the surface. This sponge like surface was noticed clearly in Figure 8.13. This micrograph didn't give the exact observation of the grain size of gel-derived Titania but they gave an idea about the grain size. It may be considered that the grain size was below 100 nm. This claim is supported by Figure 8.14 which was taken at a magnification of 20000x.
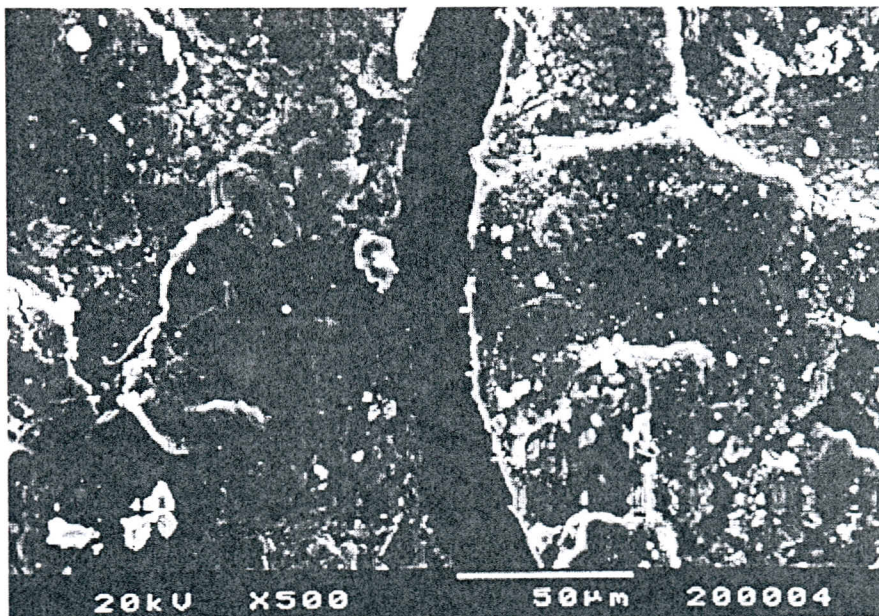

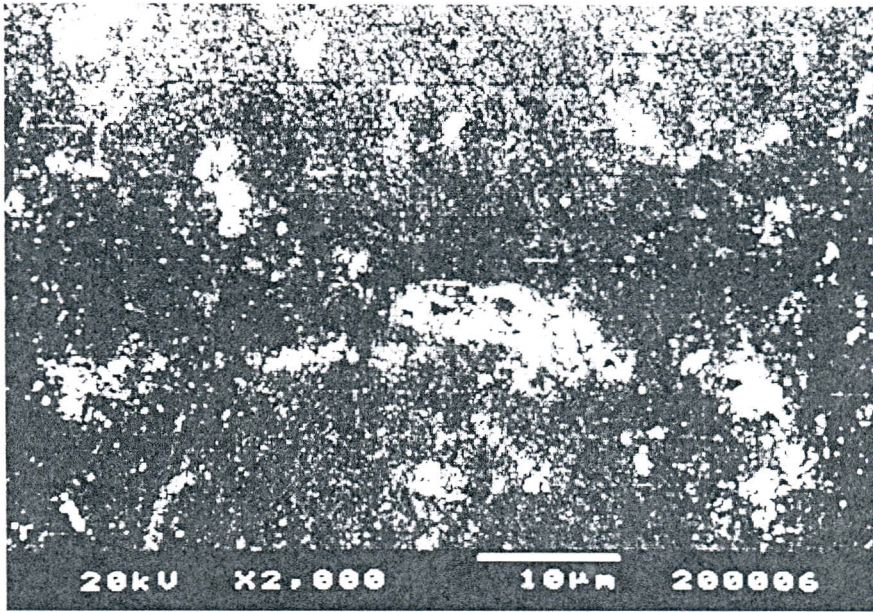Figure 8.11. The SEM micrograph of TC6 sintered at 700°C at a magification of 500x.

Figure 8.12. The SEM micrograph of TC6 sintered at 700°C at a magification of 2000x.
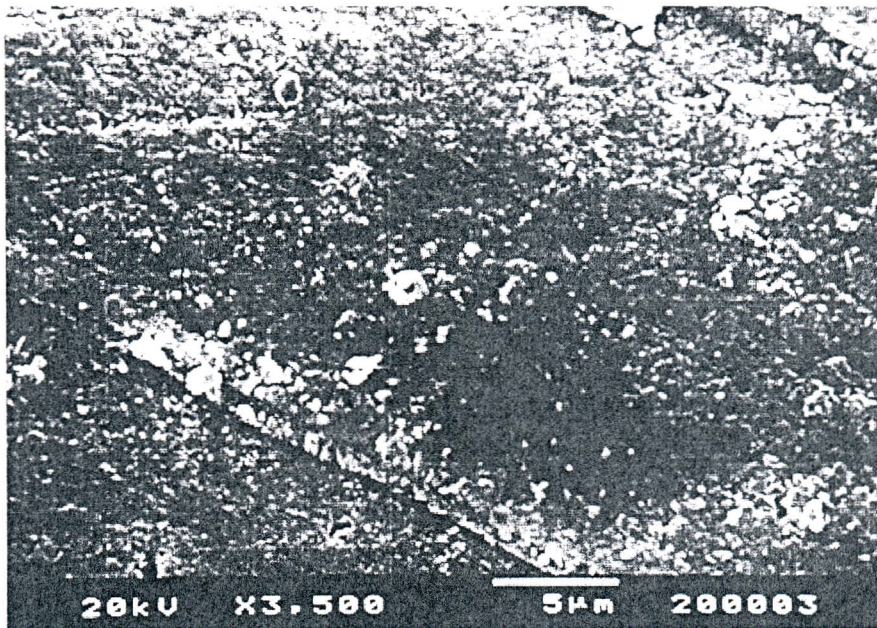

Figure 8.13. The SEM micrograph of TC6 sintered at 700°C at a magification of 3500x.
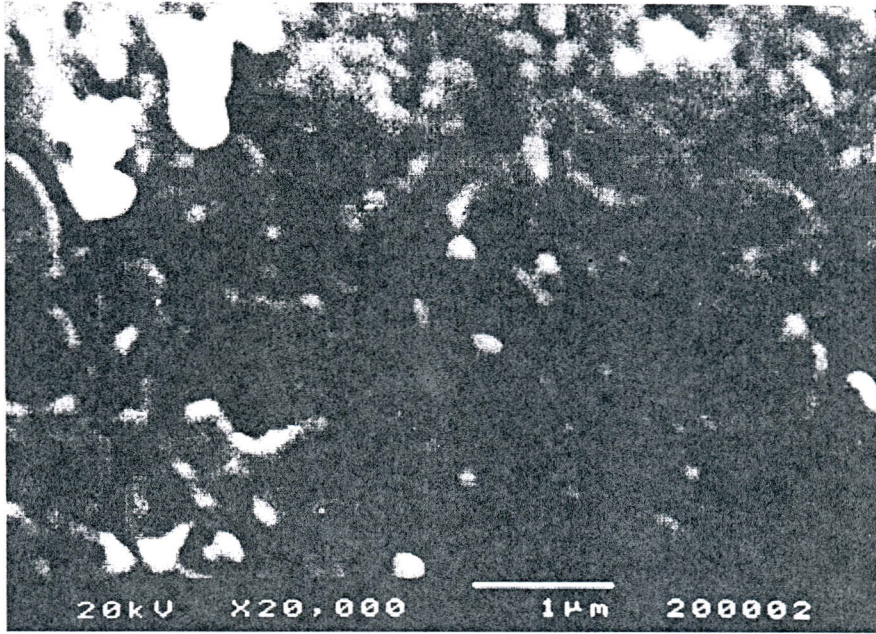
Figure 8.14. The SEM micrograph of TC6 sintered at 700°C at a magification of 20000x.

8.5. FTIR Analyses

The FTIR analyses were carried out for TC6 sols and gels with DCCAs at 1 and 2 weight percent, the produced powders and TC5 gel at different temperatures. The aim of the FTIR analyses of TC6 sols and gels was to determine the difference caused by the addition of DCCAs to the system. The FTIR spectrums of the produced powders gave the structure of them. The structural differences were observed by the FTIR spectrums of TC5 gel at temperatures between 100-900°C. The FTIR spectrums of commercial anatase and rutile titania were also achieved as reference.

FTIR Analyses of TC6 Sols: Figure 9.15 shows the FTIR spectrum of TC6 sol. The strong broad located in the region near 3300cm^{-1} owing to the stretching of O-H''O bonds may be identified as Isopropoxide. The peaks at 2960 and 2870 cm^{-1} may be caused by (RO)CH3 stretching. The medium peaks at 2400 and 230 cm^{-1} region may not be identified. The very weak peak at 1700-1600 cm^{-1} region may be C=O group. The peaks in 1640-1600 cm^{-1} and in 1560-1505 cm^{-1} may be identified as NH$_3^+$ asymmetric stretching and NH$_3^+$ symmetric stretching respectively. The weak peak at 1480 cm^{-1} was most

61

probably O-H deformation. The weak peaks at 1140 and 1030 cm^{-1} correspond to the pattern of the primary alcohols (C-O stretching). The strong broad beginning at 700 cm^{-1} was typical Ti-O broad having peaks at 540, 485, and 410 cm^{-1}. The sols with one and two weight percent oxalic acid gave some additional peaks as shown in Figure 8.16 through 8.18. The strong peaks located at 3000 cm^{-1} may be assigned as O-H stretching of the carboxyl group for TC6 sol with one weight percent oxalic acid. The strong peak located at 1400-1300 cm^{-1} region may be O-H deformation. The -C-O-C- bond of the carboxyl group absorbs in 1280-1200 cm^{-1} region. The peak in the region of 980-875 cm^{-1} may be defined as C-O deformation out of plane. The peaks identified above for the TC6 sol with one weight percent oxalic acid were shifted 5-10 cm^{-1} lower wavelengths and became stronger for the TC6 sol with two percent oxalic acid. The peak in 980-875 region was divided into two weak peaks extend to 1100-900 cm^{-1} region for the sol with two weight percent oxalic acid. The same behavior was observed for the sol with two weight acetic acid, one and two percent polyacrylic acid. This event may the result of increasing the amount of carboxyl group in the system. The peak at in 1700-1600 cm^{-1} region identified as C=O group began to have higher absorbance values as the amount of DCCAs is increased. The increase in absorbance value is explained in literature [49] as during C=O stretch vibration the electron attracting groups on the nitrogen raise the C=O frequency. This effect was clearly observed for the sols with one and two weight percent polyacrylic acid. The same peaks were located at approximately the same wavelengths and absorbance values. The small difference between oxalic acid and acetic acid may be caused by the similar structure.

FTIR Analyses of TC6 Gels: The FTIR spectrums of the all TC6 gels were slightly different than the sols. The location and absorbance values were almost the same (see Figure 8.19 through 8.22).
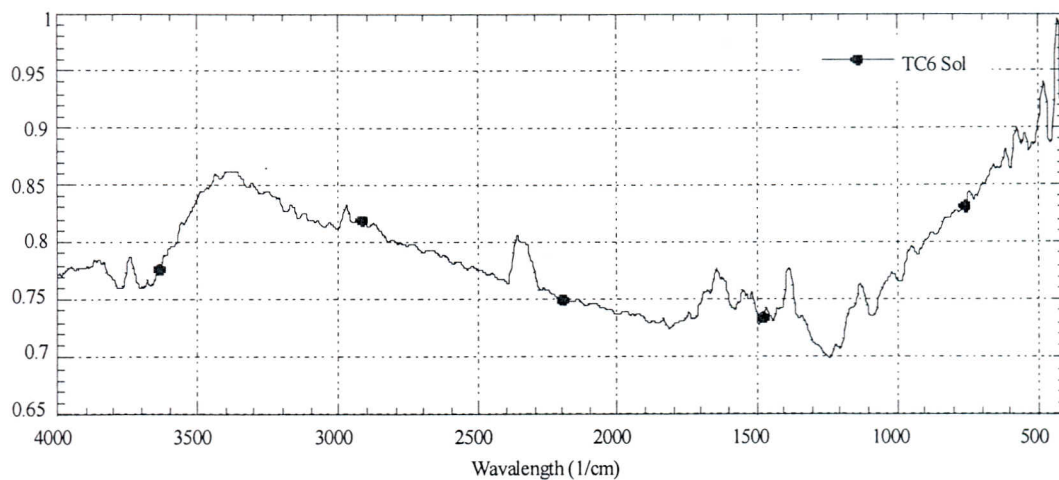

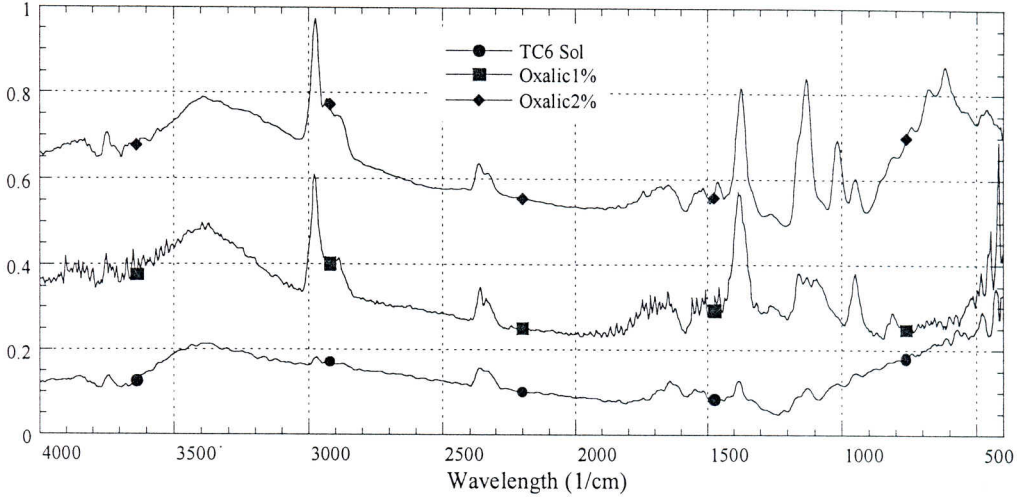Figure 8.15. FTIR spectrum of TC6 sol.

Figure 8.16. FTIR Spectra of TC6 Sol and TC6 Sols with oxalic acid at different ratios
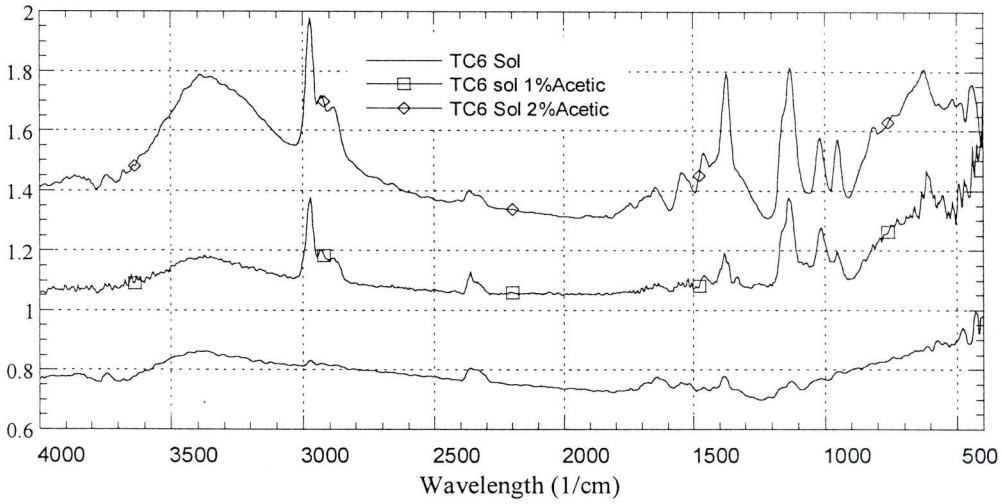

Figure 8.17. FTIR Spectra of TC6 sol and TC6 sols with acetic acid at different ratios.
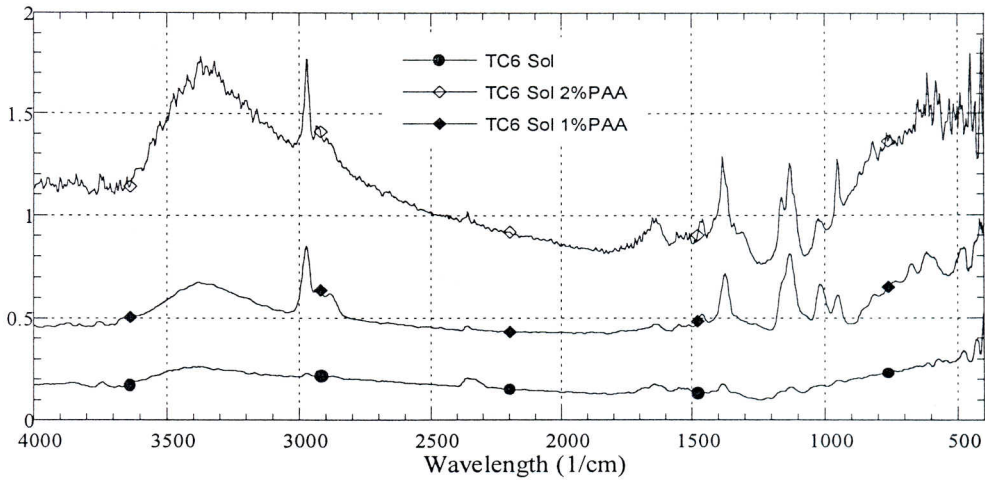

Figure 8.18. FTIR Spectra of TC6 Sol and TC6 sols with Polyacrylic Acid at different ratios.
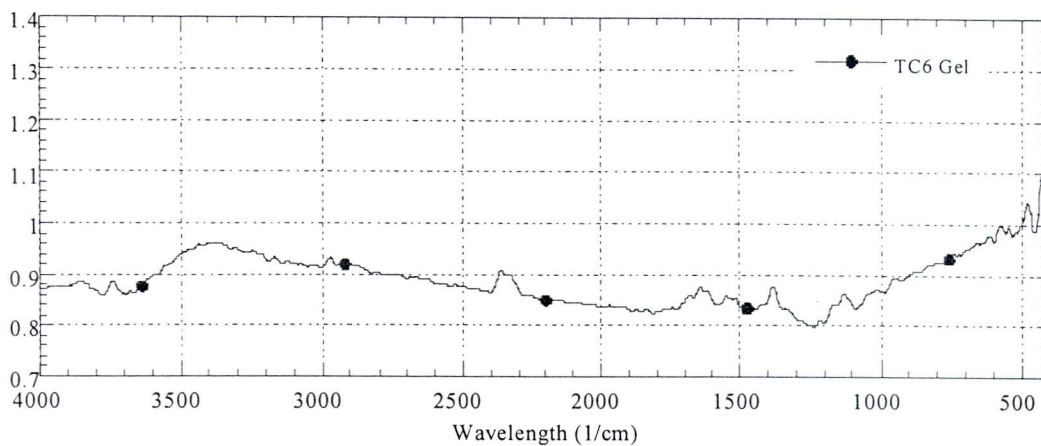
63

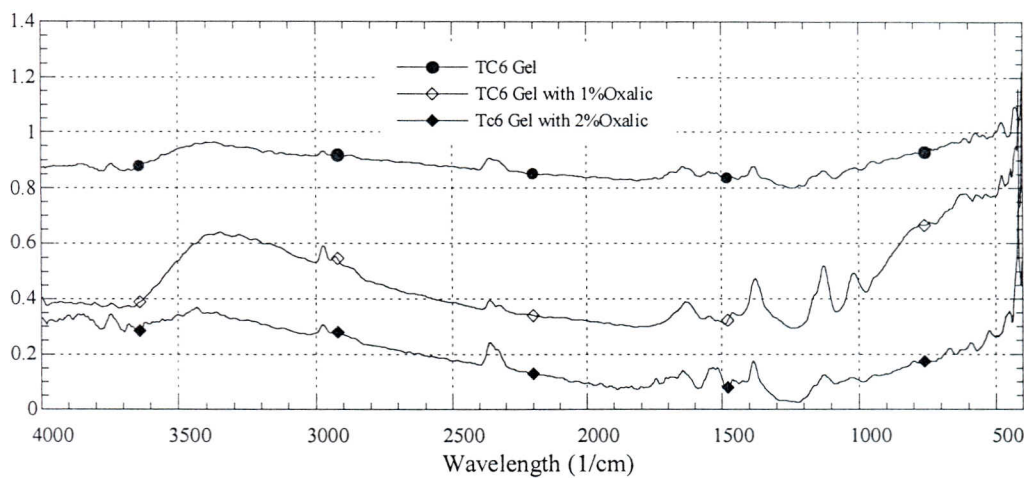Figure 8.19. FTIR Spectrum of TC6 gel.

Figure 8.20. FTIR Spectra of TC6 gel and TC6 gels with Oxalic Acid at different ratios.
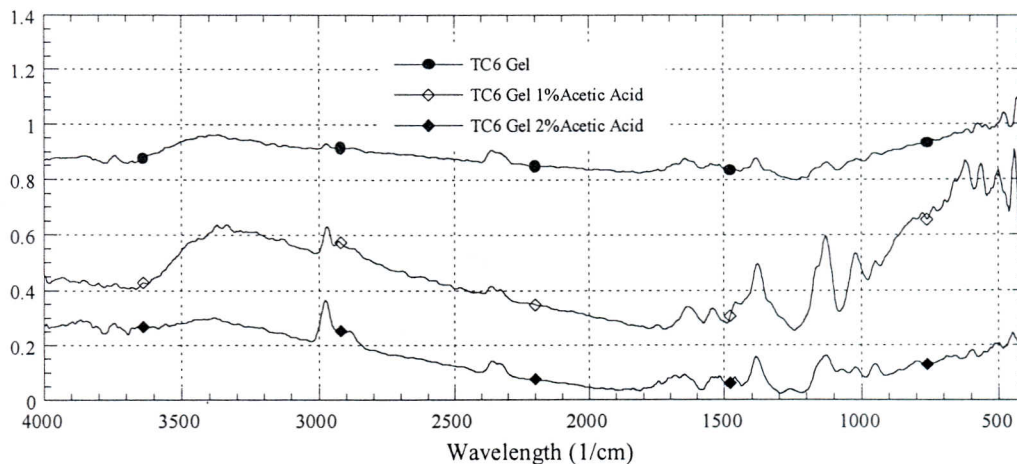

Figure 8.21. FTIR Spectra of TC6 gel and TC6 gels with acetic acid at different ratios.
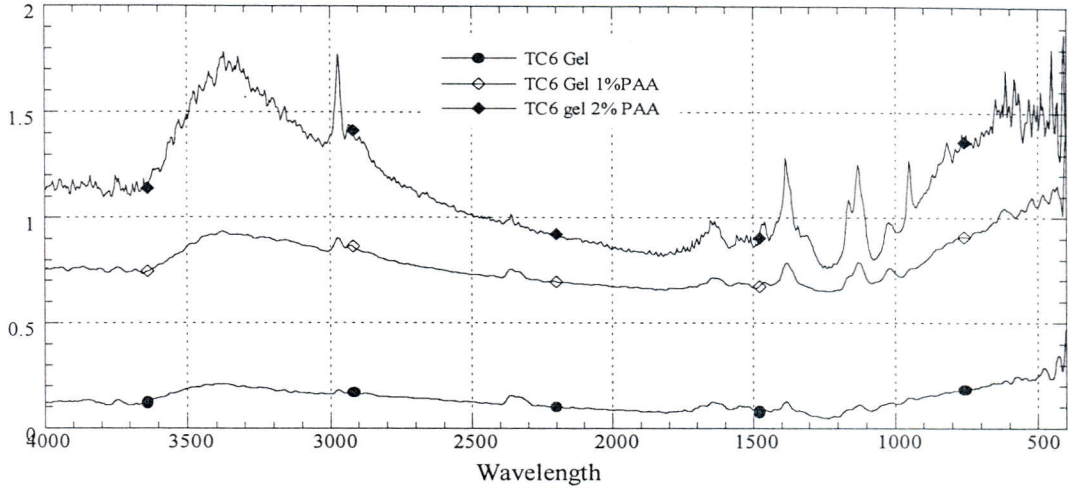
64

Figure 8.22. FTIR Spectra of TC6 gel and TC6 gels with polyacrylic acid at different ratios.
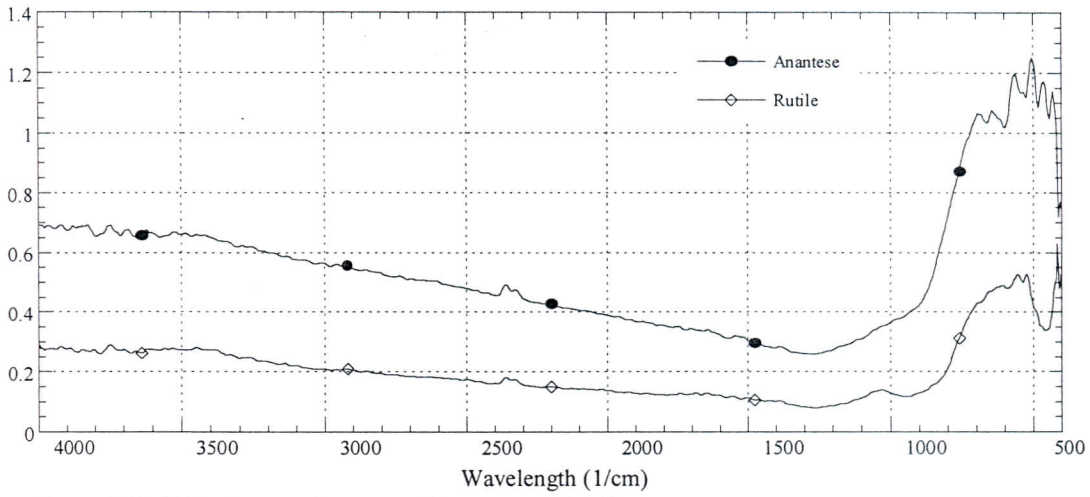

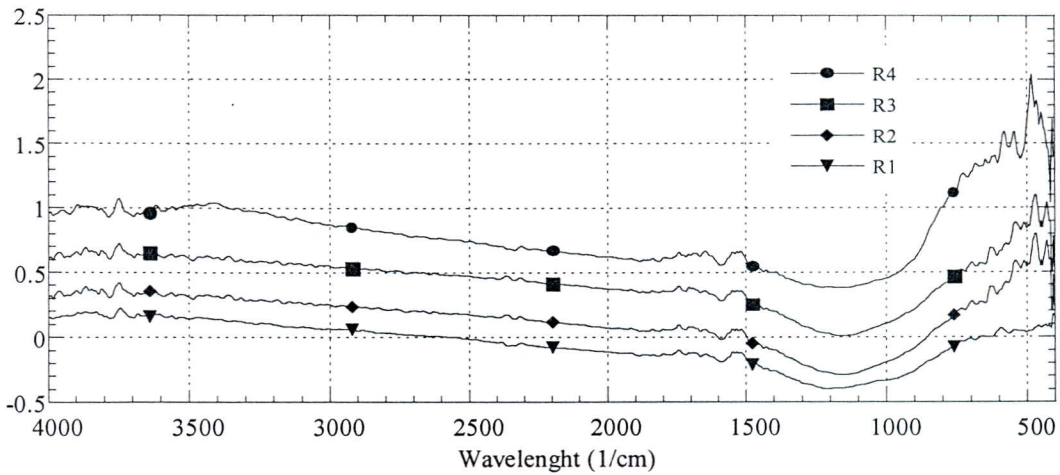Figure 8.23. FTIR Spectra of commercial anatase and rutile.

Figure 8.24. FTIR Spectra of the Route1, Route2, Route3, and Route4 powders.

FTIR Analyses of Commercial Anatase and Rutile: The FTIR spectrum of the commercial anatase and rutile titania is shown in Figure 8.23. O-Ti-O group may absorb around 700-420 cm^{-1} absorption band. The peak located at 540 cm^{-1} may show Ti-O stretching for anatase structure. The absorption band includes strong peaks at 700, 650, 550, 470 and 410 cm^{-1}. The absorption band located at 700-420 cm^{-1} may define as O-Ti-O group. The absorption band has medium peaks at 550 and 520 cm^{-1} and a strong peak at 410 cm^{-1}.

FTIR Analyses of Route 1, Route 2, Route 3, and Route 4: The all powders were calcinated at 400°C and they were thought as having anatase structure. The FTIR spectrums gave a typical anatase spectrum as shown in Figure 8.24.

FTIR Analyses of TC5: Figures 8.25 through 8.30 show the FTIR spectrums of TC5 at different temperatures. The FTIR spectrum of TC5 heat-treated at 100 °C had a strong absorption broad located around 3300 cm^{-1} may be identified as Isopropoxide absorption broad. This means that the system still had isopropoxide in the structure at 100°C. The asymmetric formation and symmetric deformation of NH_3^+ absorbs at 1625-1560 and 1550-1505 cm^{-1}. There was a strong broad in 1200-400 cm^{-1} region with a peak at 490 cm^{-1}. As it is known in literature [49] that TiO_2 has its strongest bands in the 700-500 region, the 1200-400 cm^{-1} region may be defined as O-Ti-O bonds. As temperature was increased, the broad located around 3300 cm^{-1} which was identified as Isopropoxide, it is shifted lower absorbance values and begin to smooth. At 400 °C- calcination temperature of the powders-there is no this broad located at 3300 cm^{-1}. The unidentified peak in the 2400-2300 cm^{-1} disappeared after 400C but then show up again at FTIR spectrums of TC5 at 850 and 900°C. The peaks at 1600 and 14520 cm^{-1} were identified as NH_3^+ asymmetric formation and symmetric deformation. These peaks were disappeared as the temperature was reached to 550C. The structure of Ti-O broad located in 1200-400 cm^{-1} region had changed as temperature was increased. At 300°C the typical anatase peaks began to appear. The peaks were located at 635, 515, and 410 cm^{-1}. The peak at 400 cm^{-1} appeared at 300°C. After 400°C, the peak of 515 cm^{-1} appeared. There is a sudden change in FTIR spectrums between 500 and 550°C. The FTIR spectrum of TC5 at 550°C showed a typical anatase structure which is very similar to commercial anatase. The peaks at 635, 550, 495, and 410 cm^{-1} agree with the FTIR spectrum of commercial anatase and the literature

information [27]. The anatase-rutile transformation took place at 750°C. The commercial rutile has peaks at 550, 520 and 410 cm^{-1} with a broad starting around 800 cm^{-1} as mentioned before. The sample heat-treated at 750°C has the broad band starting around 800 cm^{-1} and peaks at 615, 510, and 410 cm^{-1}. The peaks of the sample slightly differ from the peaks of the commercial rutile.

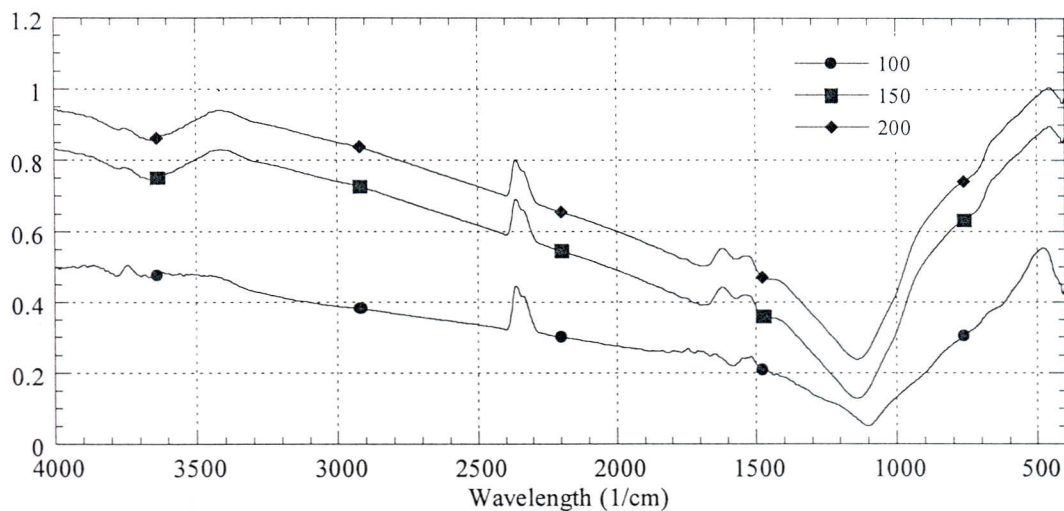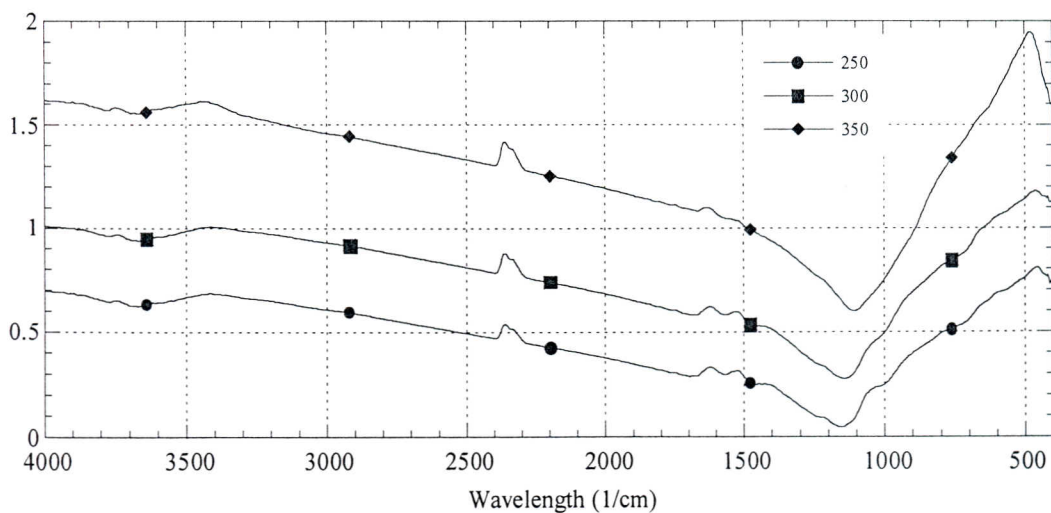Figure 8.25. FTIR Spectra of TC5 heat treated at 100, 150, 200°C.

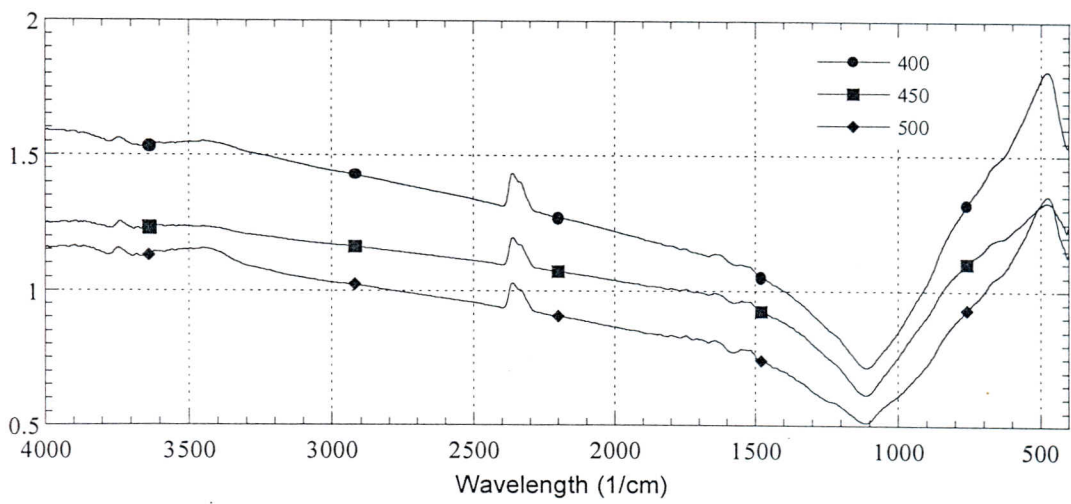Figure 8.26. FTIR Spectra of TC5 heat treated at 250, 300, 350°C.

Figure 8.27. FTIR Spectra of TC5 heat treated 400, 450, and 500 °C.
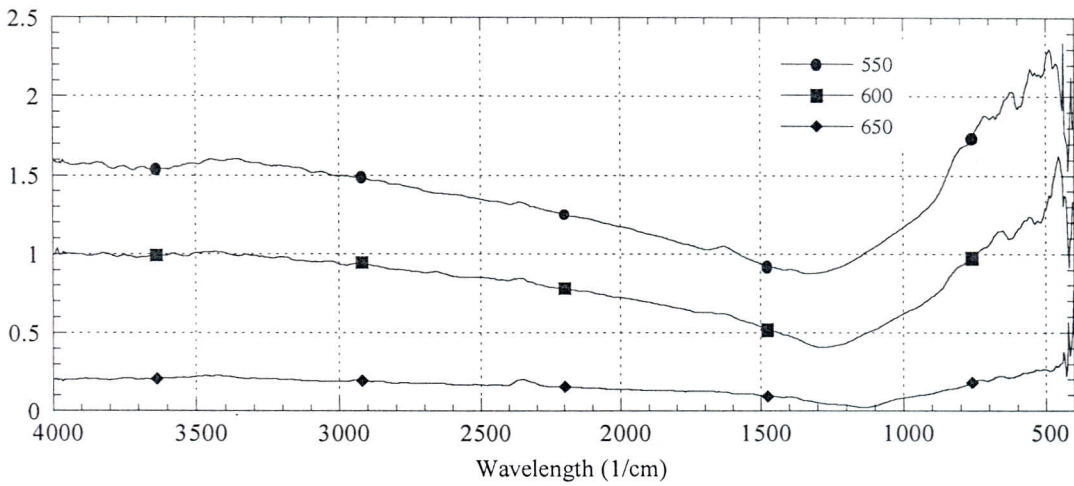

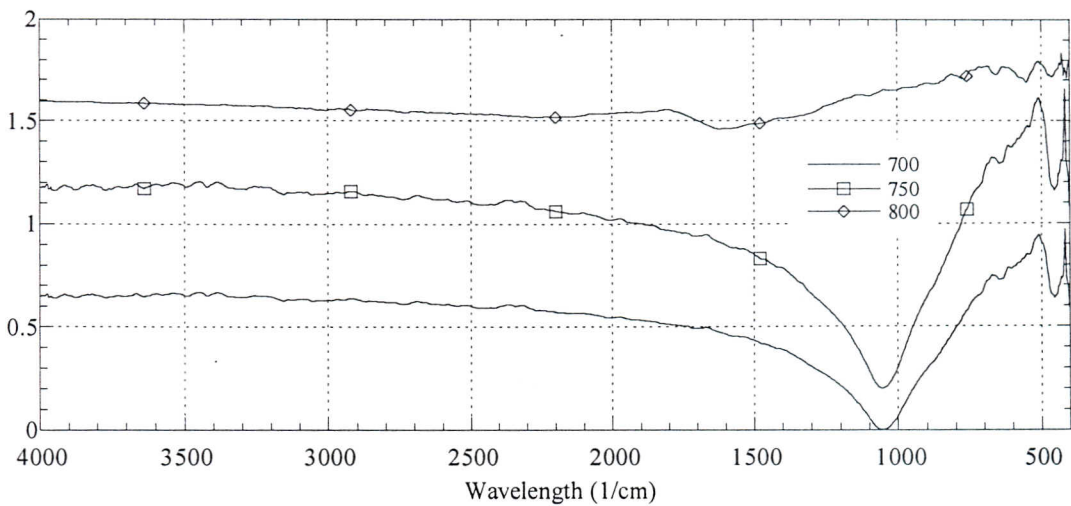Figure 8.28. FTIR Spectra of TC5 heat treated at 550, 600, and 650 °C.

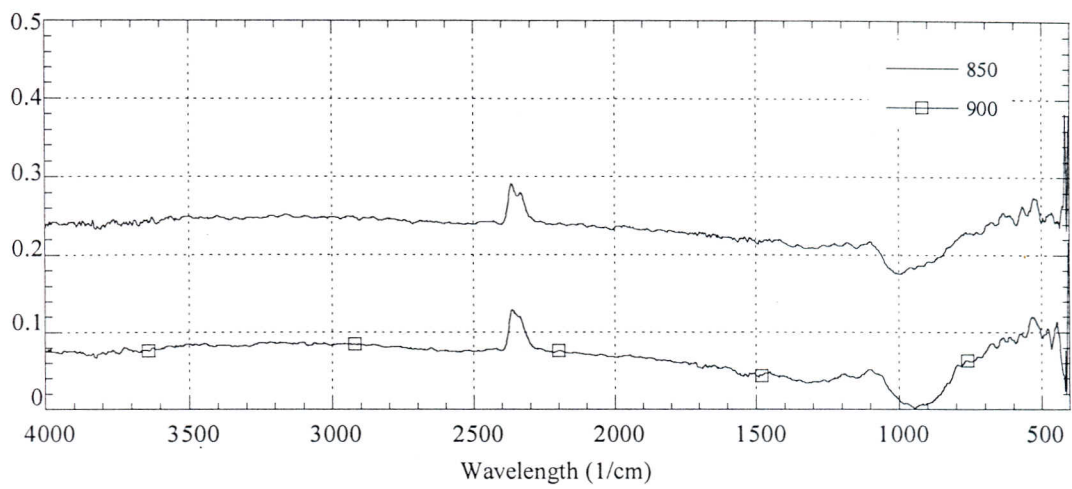Figure 8.29. FTIR Spectrums of TC5 heat treated at 700, 750, and 800 °C.

68

Figure 8.30. FTIR Spectrums of TC5 heat treated at 850 and 900°C.

Chapter IX

CONCLUSIONS

Nanocrystalline Titana were produced by sol-gel process. Two different techniques were followed. The first one is a powder-free technique that Nanocrystalline Titania were prepared by drying and subsequently sintering processes of the dried gels. The second one is a powder-based technique that is the preparation of the powder from the sols and the gels by applying different processes. The powder dry-pressed and sintered subsequently.

The dried gels and pellets were sintered at different temperatures. The densification behaviors were observed. Although the size and shape of the dried gels can not be controlled, they densified nearly their theoretical density (theoretical density of the Titana is 4.26 g/cm^3). The pore size volume of the gel show that the pores in the gels were very small (~ 35 nm) and the greenbody of the gels were calculated by using this data. The green body density of the gels approximately 70% of the theoretical density. High greenbody density and the small size of the pores might be the reasons of the high densification rate. The size and the shape of the gels could not be controlled. Some DCCAs were introduced to the sols to control the drying that generally accelerated the gelation time of the sols. But, the gels cracked during drying.

However, the pellets didn't densify as the dried gels. The main problems were the agglomeration and the compaction problems. The powders were softly agglomerated. The agglomeration problem became serious when the powder was treated in water water. Water may change the surface charge of the powder somehow and then the particles come together and agglomeration formed. The pores in the agglomerates that called, as interagglomerate pore could not reduced by dry pressing. However, the pellets had very small closed pores with relative to the open pores. This result may the indication of high-sinterability of the powders. The greenbody of the pellets are about 41-52%. There were some defects on the surface of the pellet that could be detected by visual observation. Therefore, dry pressing may not be sufficient for forming the nanocrystalline powder. Isostatic pressing or hot pressing could be use to improve the greenbody density and to minimize packing problems. As the greenbody density increases and the packing problems minimizes, better densification behavior would be observed.

The hardness test results showed that the gel pieces had significantly higher hardness strength (~1190 MPa) than the pellet's (~210 MPa). The reason of the significant difference in the hardness strength may be related with the density difference between the gel derived Titania and powder based Titania.

The SEM micrographs were taken only for the gel-derived Titania. The micrographs were not enough for showing the grain sizes accurately because of the absence of higher magnifications. However, the micrographs allowed us to estimate the grain sizes approximately. The grains were not appeared at the magnification of 20000x. If the grain sizes had been micron or sub-micron they may have been seen although the micrograph is blurry. Therefore, the expected grain sizes most likely below 100 nm.

The FTIR Spectra of the sols, the gels, and the powders gave some information about the structure of them. The FTIR Spectra of the sols and gels were approximately the same. The anatase transformation of the gels was observed at 550°C and the rutile transformation at 750 °C. However, the powders calcinated at 400°C had anatase structure.

REFERENCES

1. A. Nazeri, S.B. Qadri, Alumina-stabilized Zirconia Coatings for High-Temperature Protection of Turbine Blades, *Surface and Coatings Technology*, no.86-87, 166-169, 1996

2. A.J. Allen, S. Kruger, G. Skandan, G.G. Long, H.Hahn, H.M. Kerch, J.C. Parker, M.N. Ali, Microstructural Evolution During the Sintering of Nanostructured Ceramic Oxides, *J. of American Ceramic Society*, 79, no:5, 1201-12,1996

3. B.A. Cottom, M.J. Mayo, Fracture Toughness of nanocrystalline ZrO_2-3 mol%Y_2O_3 Determined by Vickers Indentation, *Scripta Materialia*, vol.34, no.5, 809-814, 1996

4. B.E. Yoldas, A Transparent Porous Alumina, *Ceramic Bulletin*, vol.54, no.3, 1975

5. B.E. Yoldas, Hydrolysis of Titanium Alkoxide and Effects of Hydrolytic Polycondensation Parameters, *J. Mater. Sci.*, 21, pp.1087-1092, 1986

6. B.P. Kashyap, A. Arieli, A.K. Mukherjee, Microstructural Aspects of Superplasticity (Review), *J. of Materials Science*, vol.20, 2661-2686, 1985

7. C. Carry, A. Morcellin, Structural Superplasticity in Single Phase Crystalline Ceramics, ,, vol.13, 89-98, 1987

8. D.B. Haddow, S. Kothari, P.F. James, Synthetic Implant Surfaces, *Biomaterials*, 17, pp. 501-507, 1996

9. D.W. Johnson, Nonconventional Powder Preparation Techniques, *Ceramic Bulletin*, vol.60, no.2, 221-243, 1981

10. E.A. Barringer, H.K. Bowen, Formation, Packing and Sintering of Monodisperse TiO_2 Powders, *Communications of American Ceramic Society*, December 1982

11. G.B. Kennedy, H.K. Bowen, High Tech Ceramics in Japan: Current and Future Markets, *Ceramic Bulletin*, vol.62, no.5, 590-596, 1983

12. G.W. Scherer, Aging And Drying Of Gels, *J. Non-crystalline Solids*, 100, pp. 77-92, 1988

13. G.W. Scherer, Theory of Drying, *J. of American Ceramic Society*, 73, no:1, pp. 3-14,1990

14. H. Kucukefe, The Preparation, Characterization and Sintering of Nanocrystalline Titania Powders, Thesis of Master of Science, Ege University,November 1994

15. H.Hahn, R.S. Averback, H.J. Höfler, and J. Logas, *Mat. Res. Soc. Symp. Proc.* 206, 1991

16. J. Karch, R. Birringer, H. Gleiter, Ceramics Ductile at Low Temperatures, *Nature*, vol: 330, 10 December, 1987

17. J.D. Mackenzie, D.R. Ulrich, Ultrastructure Processing of Advanced Ceramics, John Wiley & Sons, New York, 1988

18. J.L. Keddie, P.V. Braun, E.P. Giannelis, Interrelationship between Densification, Crystallization, and Chemical Evolution in Sol-Gel Titania Thin Filims, *J. Am. Ceram. Soc.*, vol. 77, no. 6, 1592-1596, 1994

19. J.S. Reed, Principles of Ceramics Processing, 2nd Edition, John Wiley & Sons, New York, 1995

20. J.-Y. Chane-Ching, L.C. Klein, Hydrolysis in the Aluminum sec-Butoxide-Water-Isopropyl Alcohol System: I, Rhelogy and Gel Structures, *J. Am. Ceram. Soc*, vol.71, no.1, 83-85, 1988

21. K. Terabe, K. Kato, S. Yamaguchi, A. Imai, Microstructure and Crystallization Behavior of TiO_2 Precursor Prepared by the Sol-Gel Method using Metal Alkoxide, *J. Of Materials Science*, vol.29, 1617-1622, 1994

22. L.S. Millberg, The Synthesis of Ceramic Powders, *J. Of Metals*, 9-13, August 1987

23. M. A. Anderson, M.J. Gieselmann, Q. Xu, Titania and Alumina Ceramic Membranes, J. Of Membrane Science, no. 39, 243-258, 1988

24. M. Ciftcioglu, M. Akinc, L. Burkhart, Measurement of Agglomerate Strength Distributions in Agglomerated Powders, *Ceramic Bulletin*, vol. 65, no. 12, 1986

25. M.F. Ashby, "A first report on Sintering diagrams", *Acta. Metallugica*, 22 (3), 275-289, 1974

26. M.J. Mayo, Ceramic-Ceramic Diffusion Bonding using Nanocrystalline Interlayers, *Nanostructured Materials*, vol.3, 163-168, 1993

27. M.J. Mayo, D.C. Hague, D.-J. Chen, Processing Nanocrystalline Ceramics for Applications in Superplasticity, *Materials Science and Engineering A 166*, 145-159, 1993

28. M.J. Mayo, D.C. Hague, The Effect of Crystallization and a Phase Transformation on the Grain Growth of nanocrystalline Titania, *Nanostructured Materials*, vol. 3, 61-67, 1993

29. M.J. Mayo, D.C. Hague, Using Superplastic Flow to Process Nanocrystalline Ceramics, *Creep and Stress Relaxation in Miniature Structures and Components, The Minerals, Metals and Materials Society*, 1997

30. M.J. Mayo, Grain Growth And The Processing Of Nanocrystalline Ceramics, *The Proceedings Of The Second International Conference*, May 1995

31. M.J. Mayo, M. Ciftcioglu, Issues in the Processing of Bulk Nanocrystalline Ceramics for Structural Applications, *Material Research Society Symposium*, 206

32. M.J. Mayo, M. Ciftcioglu, Processing of Nanocrystalline Ceramics, *Material Research Society Symposium*, vol:196, 1990

33. M.J. Mayo, Porosity-Grain Growth Relationships in the Sintering of Nanocrystalline Ceramics, *Nanostructured Materials*, vol.3, 43-52, 1994

34. M.J. Mayo, Processing of Nanocrystalline Ceramics from Ultrafine Particles, *International Materials Reviews*, 41, no.3, pp. 85-116, 1996

35. M.J. Mayo, Synthesis and Applications of Nanocrystalline Ceramics, *Center for Advanced Materials Newsletter*, vol:7, no:1, 1993

36. M.J. Mayo, Thermomechanical Stability of Nanocrystalline Microstructures and Their role in Enhancing Superplastic deformation, *The proceedings of the International Conference on Superplasiticiy in Advanced Materials*, June 1991

37. M.M. Schwartz, <u>Handbook of Structural Ceramics</u>, McGrawHill, New York, 1990

38. M.P. Harmer, E.W. Roberts, R.J. Brook, Fast Firing of Alumina Ceramics, Energy and Ceramics, *Materials Science Monographs 6*, Elsevier Scientific Publishing Company, 1980

39. M:J. Mayo, Superplasticity of Nanostructured Ceramics, Mechanical Properties and Deformation Behavior of Materials having Ultrafine Microstructures, 361-380, The Netherlands, 1993

40. P. Li, I. Kangasniemi, K. De Groot, T. Kokubo, Bonelike Hyroxyapatite Induction by a Gel-Derived Titania on a Titanium Substrate, *J. of American Ceramic Society*, 77, no:5,pp. 1307-12, 1994

41. P.P. Lottici, D. Bersani, M. Braghini, A. Montereno, Raman Scatering Characterisation of Gel Derived Titania Glass, *J. of Materials Science*, 28, pp. 177-183, 1993

42. R. S. Mishra, C.E. Lesher, A. K. Mukherjee, High-Pressure Sintering of nanocrystalline γ-Al_2O_3, *J. Am. Ceram. Soc.*, vol.79, no. −11, 2989-2992, 1996

43. R.E. Loehman, <u>Characterization of Ceramics</u>, Butterworth-Heinemann Press, Boston, 1993

44. Richard W. Seigel, Nanophase Materials Assembled from Atomic Clusters, *MRS Bulltein*, pp. 60-67, October 1990

74

45.S.J. Glass, K.G. Ewsuk, Ceramic Powder Compaction, *MRS Bulletin*, Dec., pp. 24-28, 1997

46.S.J. Wu, L.C. De Jonghe, Sintering of Nanophase Al_2O_3, *J. Am. Ceram. Soc.* vol.79, no.8, 2207-2211, 1996

47.Y.-J. Kim, L.F. Francis, Processing and Characterization of Porous TiO_2 Coatings, *J. Am. Ceram. Soc.* vol.76, no.3, 737-742, 1993

APPENDIX A

A Sample Calculation for the Sol Preparation (TC6)

Physical Properties for the Calculations:

Molecular Weight of Titanium (IV) Isopropoxide (MW_{TiISP})=284.26 g/mol

MW_{Ti}=47.88 g/mol

MW_{TiO2}=79.88 g/mol

$MW_{Isopropanol}$=60.1 g/mol

$\rho_{Isopropanol}$=0.78 g/cm³

ρ_{TiISP}=0.955 g/cm³

ρ_{HNO3}=1.036 g/cm³

6.5% 1.44M HNO_3 Acid Solution is used.

The used volume of 97% Titanium Isopropoxide for TC6 sol is 15 ml.

Constant Ratios for the Sol Preparation:

H^+/Ti=0.0537

Isopropanol/Ti=20

H_2O/Ti=2

Calculation:

n_{Ti}= (V_{TiISP}*ρ_{TiISP})/MW_{TiISP}= (15×0.955×0.97)/284.26=0.0489 mol Ti

m_{TiO2}=0.0486×79.88=3.905 g TiO_2

n_{H2O}=0.0489×2=0.0978 mol H_2O

$m_{HNO3\ Acis\ Solution}$=1.76/(1-0.065)=1.885 g HNO_3 Acid Solution

V_{HNO3}=1.885/1.036=1.82 ml HNO_3

N_H^+=1.82×(1.44/1000)=2.63 10^{-3} mol

H^+/Ti=2.63 10^{-3}/0.0489=0.0537 √ (the ratio controlling)

Ispropanol/Ti=20 $\Rightarrow$ $n_{Isopropanol}$=20×0.0489=0.978 mol Isopropanol

$V_{Isopropanol}$=($n_{Isopropanol}$*$MW_{Isopropanol}$)/$\rho_{Isopropanol}$=(0.978×60.1)/0.78=75.36 ml Isopropanol

$M_{Isopropanol}$=0.978×60.1=58.78 g Isopropanol

M_{Total}=(15×0.955)+1.885+58.78=74.99 g TC6 Sol

Ti wt%=(3.905/74.99)×100=5.21 wt% TiO_2 in the sol

Sample Calculations for the Density Measurements

1. *Density measurement calculation for non-porous sample:*

$$\rho^* = \left(\frac{Wd - (\rho_{fluid} - 0.0012)}{0.99983 \times G} \right) + 0.0012$$

2. *Density measurement calculation for porous sample:*

$$\rho^{**} = \left(\frac{Wd \times \rho_{fluid}}{Ws - Wss} \right)$$

3. *Relative density calculation:*

$$RD\% = (\rho_S / \rho_{THEO}) \times 100$$

4. *Open pore percent calculation:*

$$O.P. = \frac{(W_S - W_S) / \rho_{FLUID}}{W_D / \rho_{SAMPLE}}$$

W_D= Dry Weight of the sample (1)

G= Weight in water with out any process (2)

W_S= Saturated weight (1) (The sample is kept for half of an hour in boiling water then it let to cool in water. The liquid film is removed with a wet handkerchief and measurement is done)

W_{SS}= Weight in water after the process (2)

ρ_f = Density of water

ρ_S= Density of sample

ρ_{THEO}= Theoretical density of the sample

APPENDIX B

Table : Pore Size Distribution Analyses Results.

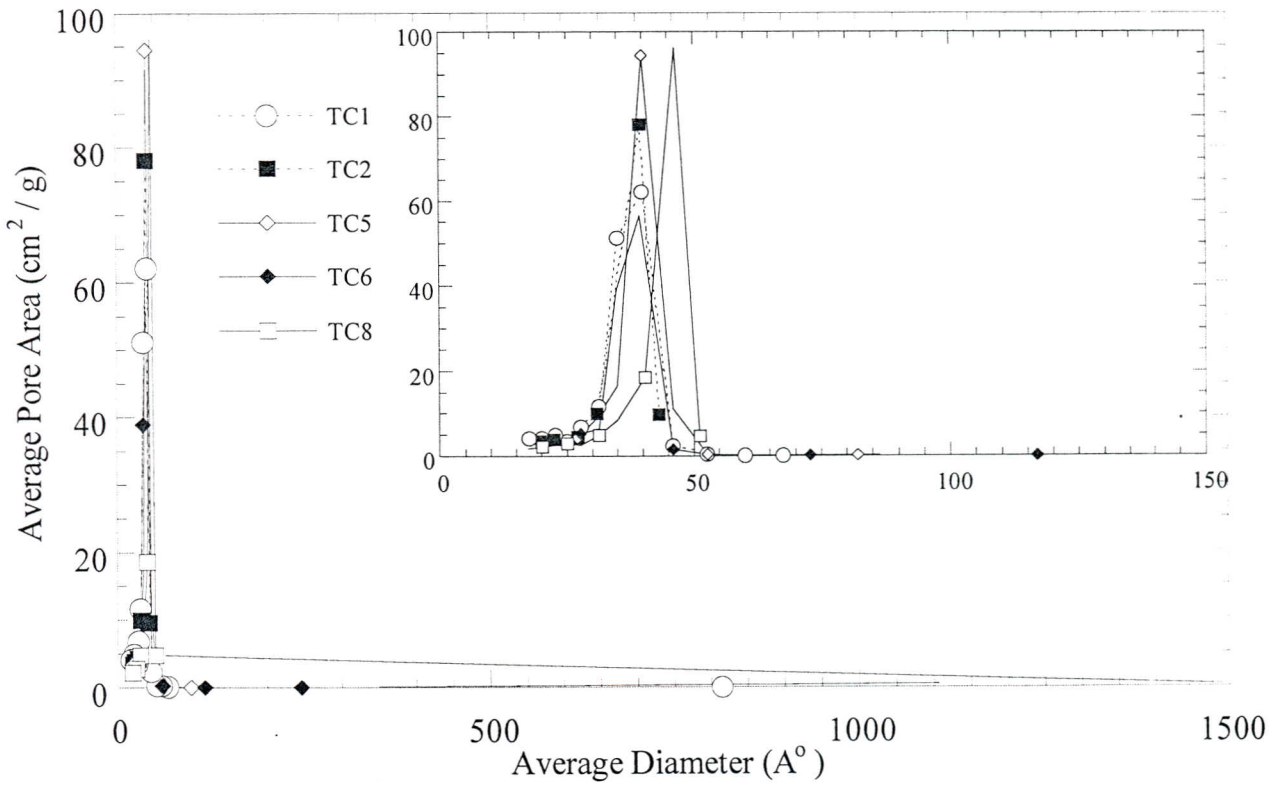|	TC1	TC2	TC5	TC6	TC8
BET Surface Area (m^2/g)	104.91	95.01	99.01	83.76	99.04
Langmuir Surface Area (m^2/g)	154.39	118.60	121.37	117.82	126.52
Average Pore Diameter by BET (Å)	49.50	54.16	56.22	50.32	60.54
Average Pore Diameter by BJH Adsorption (Å)	41.61	43.51	48.88	43.01	50.62
Average Pore Diameter by BJH Desorption (Å)	35.18	36.57	40.54	35.61	45.53

Figure 8.4. The pore area distribution of TC1, TC2, TC5, TC6, and TC8 gels.